



POLITECNICO DI TORINO

Corso di Laurea Magistrale in Ingegneria Energetica e Nucleare

Tesi di Laurea Magistrale

**Preliminary study of liquid metal stability for  
a fusion reactor divertor target using a  
capillary-porous structure**

**Relatore**

Prof. Fabio SUBBA

**Correlatore**

Ing. Giuseppe Francesco NALLO

**Candidato**

Roberto Silvestro



# Contents

<b>1 Abstract .....</b>	<b>5</b>
<b>2 Introduction .....</b>	<b>7</b>
2.1 Fusion energy.....	7
2.2 The DTT and power exhaust problem .....	10
<b>3 The role of the divertor in fusion reactors .....</b>	<b>13</b>
3.1 Introduction.....	13
3.2 Divertor concepts .....	15
3.2.1 Solid ITER-like divertor.....	15
3.2.2 Choice of the liquid metal .....	16
3.2.3 Liquid metal divertor designs.....	18
3.2.3.1 Introduction .....	18
3.2.3.2 An example of flowing liquid metal divertor: LiMIT .....	19
3.2.3.3 The capillary porous structure concept.....	20
3.2.3.4 Vapor box .....	21
<b>4 Aim of the work .....</b>	<b>23</b>
<b>5 Problem definition and preliminary calculations .....</b>	<b>25</b>
5.1 Pressure balance.....	25
5.1.1 Capillary pressure .....	26
5.1.2 Pressure drop at liquid-vapor phase transition.....	27
5.1.3 Hydrodynamic and hydrostatic pressure drop .....	28
5.1.4 Plasma pressure and pressure in supply system.....	29
5.1.5 Pressure drop due to magnetic field interaction.....	30

<b>6 The model</b> .....	<b>33</b>
6.1 Preliminary calculations .....	33
6.1 2D thermo-electric model .....	36
6.1.1 Thermal model .....	38
6.1.1.1 Grid independence for temperature .....	41
6.1.2 Electric potential model .....	42
6.1.2.1 Electric model benchmark and TEMHD contribution .....	44
6.1.2.2 Grid independence for potential .....	48
<b>7 Results</b> .....	<b>49</b>
7.1 Parametric study on pressure contribution.....	49
7.2 Comparison among pressure contributions for a reference case .....	56
<b>8 Conclusions</b> .....	<b>58</b>
<b>9 References</b> .....	<b>59</b>

# 1 Abstract

The issue of power exhaust in fusion reactors is currently considered as one of the potential show-stoppers on the pathway towards the realization of fusion energy. As the power of fusion devices increases (from current experiments to the foreseen demonstrator reactor DEMO), also the specific load on the divertor -the component which is responsible for exhausting the power- increases. Under such conditions, the currently envisaged baseline divertor design -based on actively cooled tungsten monoblocks- would have a lifetime of less than two operation years, forcing the fusion power plant to be shut down for maintenance for a relatively long time. For nuclear fusion electricity to be competitive, this would be unacceptable.

One of the alternatives to this baseline strategy is to employ a liquid metal (LM) divertor. The working principle consists in keeping in place a thin film of liquid metal in the region where the plasma ions and electrons imping, i.e. the divertor targets. Exposing a liquid surface to the plasma would avoid issues associated with melting. Moreover, concerns about thermomechanical stresses could be relaxed. The issues of power handling and of neutron compatibility could be decoupled (the plasma-facing surface would be the molten metal, whereas the substrate on which the LM film is placed could be designed optimizing the compatibility with the high neutron fluences foreseen in the reactor). Moreover, both the LM evaporation and the interactions of the evaporated metal with the near-divertor plasma could reduce the heat to be exhausted by the component.

Among the difficulties associated with the implementation of an LM divertor, we can cite issues associated with the LM surface and with the plasma response to the presence of the divertor. From the point of view of the surface, confining an LM film in an environment with extremely large magnetic fields is a challenge. It is also necessary to constantly replenish the surface to compensate for the material erosion associated with evaporation and sputtering by plasma ions. To face these challenges, it has been proposed to employ a Capillary-Porous Structure (CPS) to hold the LM in place, avoiding droplet emission and providing passive replenishment -in a similar way as it is done in heat pipes-. From the plasma physics point of view, it has been mentioned that the evaporated metal interacts beneficially with the near-

divertor plasma, since it allows to exhaust part of the heat load via line radiation and Bremsstrahlung. Nevertheless, should the metal radiate in the core plasma or excessively dilute it, the fusion reactor performances would be heavily reduced.

This thesis is focused on theoretically assessing, based on literature data and simple calculations, the capability of the CPS to hold the LM in place. To this aim, a detailed pressure balance for the LM in the CPS has been performed. Various terms of the balance are evaluated based on conditions expected in a fusion reactor. The simplicity of the model allows for performing fast parametric scans, thereby grasping the effect of design choices and of reactor operating conditions on the LM confinement.

## 2 Introduction

### 2.1 Fusion energy

The growth of the world population implies an increasing electrical energy demand. Nuclear fusion has the potential to provide a solution to this demand which is compatible with the requirement to drastically reduce the CO<sub>2</sub> emissions in the atmosphere. Nuclear fission and fusion reactors have indeed in common the fact of being essentially CO<sub>2</sub> neutral. Moreover, both reactor types have the potential to represent a reliable contribution to the base load of electric supply. Fusion reactors have the advantage of being more acceptable from the point of view of the public opinion due to the less significant production of radioisotopes.

Fusion energy relies on the binding energy per nucleon of the atoms interacting in the fusion reaction [1].

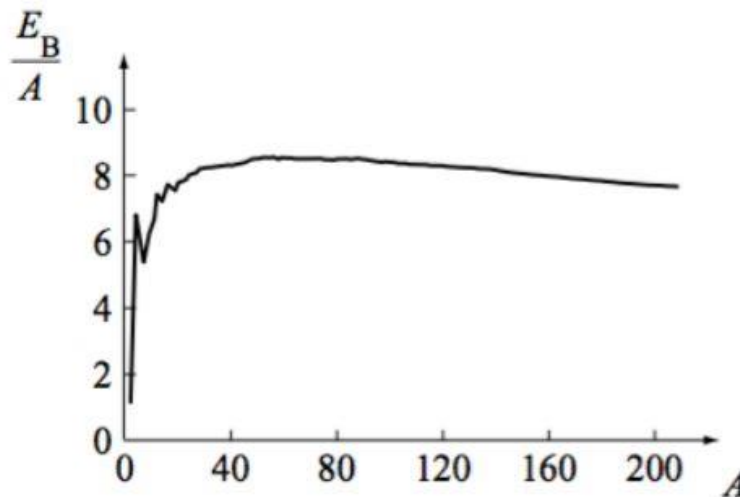
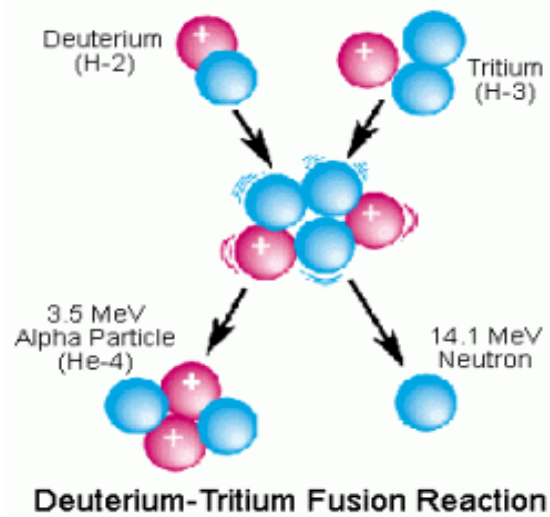


Figure 1: Binding energy [MeV] per nucleon vs mass number -  $A=2$  for Deuterium and  $A=3$  for Tritium- [1].

The most favorable fusion reaction, according to the condition achieved in current fusion experiments and foreseen at least for the first generation of fusion reactors is the one between Deuterium and Tritium. “Most favorable” indicates that the fusion reaction cross section at the relevant plasma temperatures is larger with respect to other possible reactions, e.g. Deuterium-Deuterium.



*Figure 2: Deuterium-Tritium fusion reaction products, with their energies indicated, adapted from Wikipedia.*

Thermonuclear fusion requires a collection of ionized atoms, called plasma, to be kept at around 10 million degrees. The plasma is confined by a magnetic field that keep it detached from vessel components to prevent damage to the plasma-facing components (PFCs) and contamination of the plasma itself. The confinement is fulfilled by employing coils that provide an inductive magnetic field generated by the electric current flowing into them; those coils are arranged around the toroidal shaped vessel that envelop the plasma as figure 3 shows, a toroidal field is exploited to ensure system stability, a poloidal one to provide the confinement and a vertical field is used to counterbalance arising forces due to geometry providing equilibrium and shape refining.

The alpha particles arising from fusion reactions are in turn confined by magnetic fields, and therefore contribute to heat the plasma, hence sustaining the temperature. The Neutrons instead escape the confinement and end their path being collected along with their kinetic energy in the blanket, they are exploited to heat up the coolant and in tritium breeding processes.

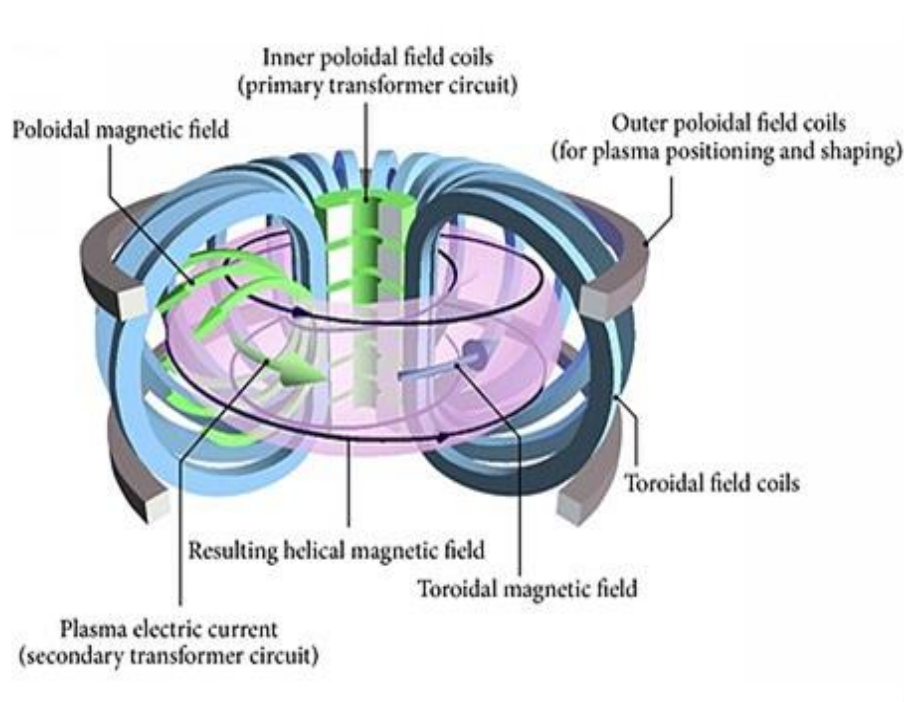


*Figure 3: schematic representation of a tokamak magnetic field and coils adapted from euro-fusion website.*

The fusion reactors arranged in the aforementioned configuration are called tokamaks (a Russian acronym for *toroidal'naya kamera s magnitnymi katushkami* translated as toroidal chamber with magnetic coils)[1]. It has to be pointed out that other reactor concepts exist such as the stellarator [1] that do not drive a plasma current. Other ways to achieve fusion favorable condition are also being considered, such as the so called inertial confinement [2]. Among these technologies, the most promising and widely studied is the tokamak.

Tokamak machines are already operating, with research purposes in physics and technology, close to reactor-like conditions. To cite just a few of them: the JET built in Oxfordshire England in 1984, ASDEX upgrade at Max Plank institute for plasma physics in Garching, Germany and WEST, once TORE SUPRA, one of the most recent machines situated in Cadarache, France.

ITER, is the next-generation fusion experiment. It is under construction in Cadarache (FR). It is expected to link the actual knowledge in fusion-engineering and physics acquired with currents tokamak fusion experiments to a steady operating condition. The first demonstration of a fusion reactor concept will be DEMO. It will supply electricity to the grid, whose project is still under design.

## **2.2 The DTT and power exhaust problem**

To provide the framework for this thesis, it must be mentioned that ITER is intended to bridge many, but not all, the knowledge-gaps required for realizing DEMO. As far as the plasma is concerned, it will address thoroughly issues like plasma confinement, stability and transport. Nevertheless, the smaller size and the less challenging operating conditions are such that other aspects needs to be faced by mean of a side project. The project is represented by the divertor tokamak test facility or DTT, which is being designed in Italy and is intended to deal mainly with the power exhaust problem [3]. The DTT will be realized in Frascati (IT) and will start operating more or less at the same time as ITER.

The power exhaust problem is related to particles that escape the plasma magnetic confinement causing impurity sputtering and high heat deposition on the PFCs. In fact, charged particles manage to flee the confinement through collisional events exploiting the negative particle density gradient towards higher minor radius and enter the so called scrape-off layer (SOL) - the edge plasma region between the last closed magnetic surface (LCMS) and the plasma facing components of the chamber -. Even if their motion is mostly prevented across the magnetic surfaces, they can freely move along them. As a results the strike point of all the charged particle that enters SOL will be a localized spot of huge heat and particles deposition. The heat and particle loads are associated to the convergence of ions spiraling around the magnetic lines beside the LCMS.

The magnetic lines shape in the SOL focus a suited region, built on purpose to mitigate and withstand very high thermal and particle load, the divertor. This profile of the magnetic field

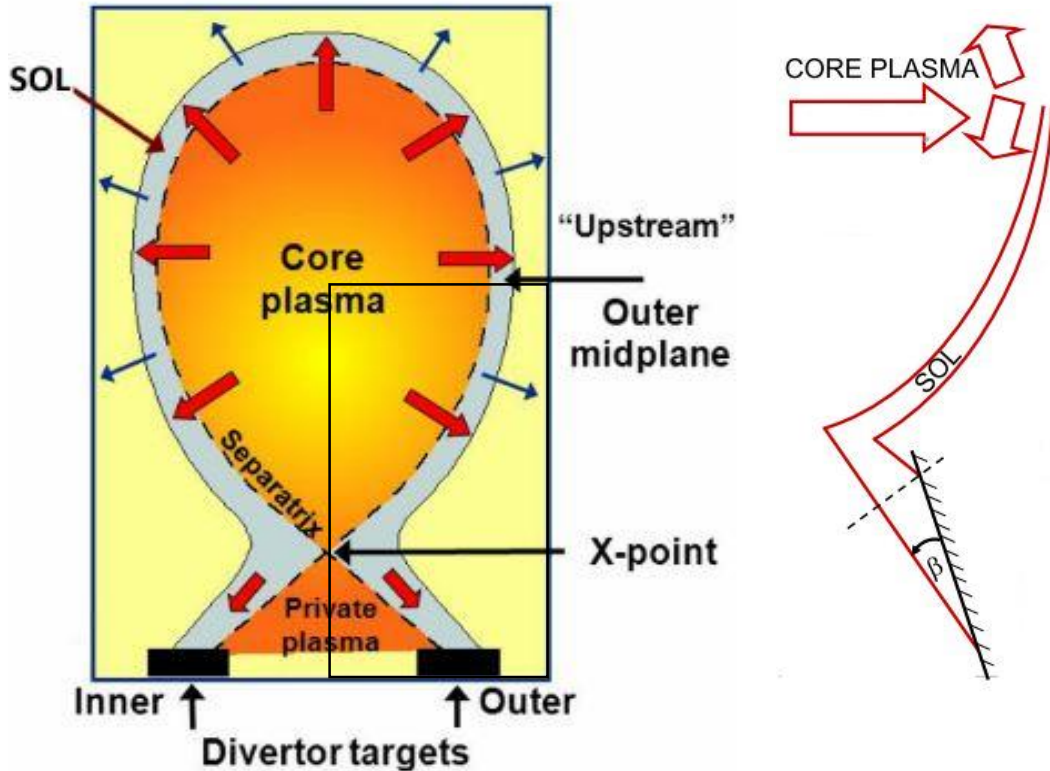


Figure 4: schematic view of the poloidal section of a single null tokamak adapted from [11] on the left and a magnify of the region of interest on the right.

lines is created adding a coil underneath the torus that modify the magnetic field in order to create an X-point (Single Null configuration) in the poloidal section as figure 4 shows, forcing the magnetic surfaces outside the LCMS to imping on the divertor.

To reduce the Heat load to the divertor targets, other magnetic configurations are studied. Possible ideas are to create additional strike points (Double Null configuration) or to increase the plasma-wetted area (XD configuration) [4]. The single null configuration is the reference for this work since it undergoes the heaviest load.

Neutrons instead follow a different path, they propagate isotropically due to the lack of charge and there is no mean to interact with them by mean of magnetic fields, therefore they spread evenly on the vessel surface releasing their kinetic energy into the blanket.

During steady operating condition ITER divertor plates have to dissipate a peak load ranging from 5 to 10 MW/m<sup>2</sup>. For DEMO, the heat load is expected to be 3-4 times higher. Moreover the displacements per atom (dpa) are foreseen to be up to 30 times larger than for ITER [5]. This discrepancy is sufficient to make the divertor designed for ITER with solid tungsten plates unsuitable for DEMO standards, due to the degradation that solid metals undergo caused by cracking phenomena, erosion, melting and embrittlement. The mechanical properties of the device are not preserved and structural stresses enhance the process. Moreover, Tungsten sputtering from the plate leads to the contamination of the plasma through high radiative particles, potentially preventing the fusion reaction to reach a self-sustained condition.

Therefore, to study and assess the most suitable divertor design for DEMO the DTT facility is envisioned [6], [7]. This facility is meant to develop and test controllable power exhaust solution for DEMO including plasma, PFCs, control diagnostics/actuator, trying to answer along with ITER to the questions that will lead to a successful DEMO project.

## 3 The role of the divertor in fusion reactors

### 3.1 Introduction

As introduced in section 2.2 inside the plasma there is a gradient in particle density. Particles may cross magnetic surfaces thanks to collisional events and be scattered over it. Inside the inner zone, next to a magnetic surface, with a higher density of particles, there will be more collisions than in the outer one; as a result of this effect a net outflow of particles arises. Tracking further these particles, when they came across the LCMS and enter the SOL, they have a very short time to advance in the radial direction through collisions. In fact, the preferential moving direction is the one along the magnetic field lines and their velocity is equal to the local sound speed [8]. As a result, the majority of the particles crossing the separatrix will end their path impinging on the divertor plates.

The most beneficial working condition for a fusion plasma is called H-mode (high confinement mode)[9]. In this condition, plasma parameters are enhanced, broad density and temperature profile are reached and the energy confinement time (that define the time needed to drain all the plasma energy through power losses) can be up to 2-times higher than the one of a plasma operating in L-mode (low confinement mode). This latter mode is characterized by turbulence in the edge plasma, that enhances transport and flattens the edge profiles.

In order to reach the favorable H-mode condition it is necessary to increase the edge plasma electron temperature over certain limits [10]. This will cause the minimum power entering the SOL,  $\sim 100\text{MW}$  in ITER, to be a lower limit for the divertor load. Moreover, the H-mode is characterized by periodical instabilities, called ELMs (edge localized modes); these are macroscopic disruption in the H-mode barrier region, that discharge a few percentage points of the plasma stored energy arising heavy transient load for the PFCs and mainly the divertor. Has to be mentioned that some modes avoiding ELMs formation have been achieved, such the so called QH-mode (Quiescent H-mode), but the absence of ELMs favors impurities to pile up into the plasma worsening its status.

The divertor is then the most significantly loaded component in terms of heat flux and particles; the deposition on the plates of the kinetic energy of each particle, that has a temperature of few eV, will result in a load of tens of  $\text{MW}/\text{m}^2$ . Even with all the precautions

to spread the load on a wider area, tilting the plates at a shallow angle with respect to the magnetic field lines, the most involved area in the poloidal section is just of few centimeters. The capability of the component to dissipate and withstand such load is therefore crucial. The particles sputtering is responsible for the deterioration of the divertor plates and it will trigger two effects: 1) the divertor performances can be worsened through erosion and embrittlement of the plates; 2) the eroded particles can contaminate the plasma dissipating heat through nuclear interactions of their electrons with the plasma (by ionizing or Bremsstrahlung radiation).

A helpful parameter that well highlights the condition in the region immediately further the LCMS, that strongly affect divertor design, is the power width  $\lambda_q$ . It defines the characteristic length of the exponential decay that the power undergoes in the radial direction. The wider it is the most the power entering the SOL will be spread, favoring less harsh condition on the divertor surface. For ITER it not even 5mm. Moreover,  $\lambda_q$  is inversely proportional to the plasma current  $I_p$  [11], that grows with reactor power. Below, a correlation proposed by Goldston [12], considered to be one of the best estimate, at present, for the power width.

$$\lambda_q = 5671 \cdot P_{sol}^{1/8} \frac{(1 + k^2)^{5/8} a^{17/8} B^{1/4}}{I_p^{9/8} R} \left( \frac{2\bar{A}}{\bar{Z}^2(1 + \bar{Z})} \right)^{7/16} \left( \frac{Z_{eff} + 4}{5} \right)^{1/8} \quad (1)$$

The key features that a well-designed divertor has to fulfill are: the capability of handling powers of tens of MW/m<sup>2</sup> and of minimizing the impurities sputtered into the plasma, in order to guarantee a high degree of purity (identified by the effective ion charge parameter or  $Z_{eff} < 1.5$ ); a long durability, associated with the capability of withstand transients without relevant damage and recover to steady state condition; a low affinity with tritium to avoid excessive retention. A last remarkable feature is to guarantee a sufficient particle exhaust avoiding hazardous build up onto the PFC.

Many divertor proposal are being screened recently; in the following section some of them are briefly presented.

## 3.2 Divertor concepts

### 3.2.1 Solid ITER-like divertor

In the divertor project WPDIV of the EUROfusion Consortium are studied several different design concepts of target PFC [13]. Most of them share some common features that are enlisted below.

Each divertor “tile” an array of rectangular monoblocks of tungsten with a cooling pipe running through them in the center as figure 5 shows. The monoblock may slightly change shape among the various designs trying to mitigate plastic deformation due to thermal stresses. The tungsten armor and the copper alloy pipe (or his composite CuCrZr) are a constant in each design of this kind, as well as employing water at around 130°C as baseline coolant inlet temperature, since it is the lowest acceptable value to avoid severe embrittlement of the Cu layer by neutron irradiation, an eventual gas cooling proposal is left only as an optional case of study for long term development.

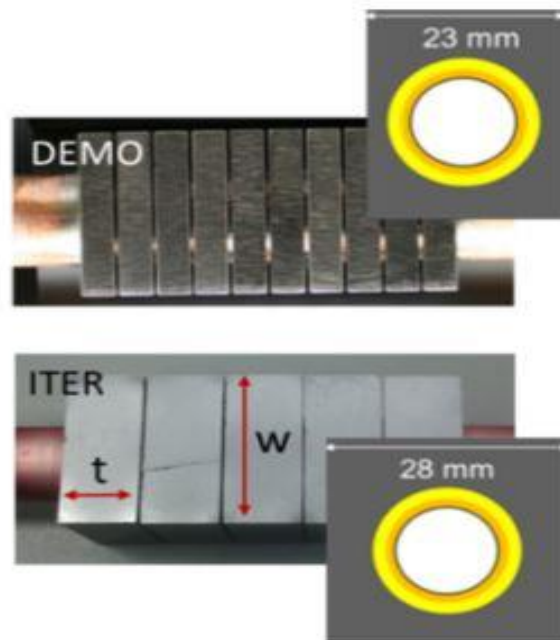


Figure 5: tungsten monoblocks, DEMO and ITER variants, adapted from [13].

The thickness of the armor ranges from an initial 5mm up to 8mm in the latest designs. Standard width and diameter respectively of the monoblock and pipe range around 23mm the first and 12mm the conduit with an interlayer thickness of 1.5mm.

Due to the harsh condition that it has to withstand, the expected lifetime of this component is around 2 full-power years. Thermal stress fields analysis at around 20 MW/m<sup>2</sup> heat flux, show that this condition exceeds the tolerable operation limits. Temperatures excursion are so strong that strains due to different thermal expansion coefficient between tungsten and copper will cause degradation.

A proper material solution is therefore still under development. A beneficial countermeasure is to reduce the monoblock dimensions to relax the structural thermal strain. However, lifetime limit associated to erosion will in this case become more severe. Others solutions are also being proposed trying to fit in the narrow acceptability band between thermal stress and embrittlement limit.

### **3.2.2 Choice of the liquid metal**

The choice of the best liquid metal is still open due to the great number of criteria to be satisfied and the necessary trade-off performed among the different alternatives.

The required features are a strong surface tension (to restrain splash damage), a low atomic number  $Z$  (since this is linked to a lower contamination rate per particle), an adequate material compatibility with regards to corrosion, wetting and chemical stability with others component materials that it can come in touch with, low activation by neutron flux, a low vapor pressure to limit evaporated metal outflow that leads to plasma dilution and contamination, a high latent heat to increase heat dissipation through evaporation and a low tritium retention [5].

The debate settled up around lithium or tin or a combination of the two [14]. Lithium has been the most studied since the liquid metal concept was introduced. It has a low atomic number ( $Z=3$ ), meaning that even a significant amount of lithium can be tolerated in core plasma, has a good wettability that helps capillary pressure to be dominant. In the early stages, lithium has been mainly chosen thanks to its ability to operate in a low recycling regime, which is highly beneficial for plasma performance. Unfortunately, for temperatures

higher than 450°C it loses this feature, but on the other hand a high recycling divertor means an overall lower temperature in the diverted zone due to the high ionization rate of the neutrals heading towards the plasma, so there are conflicting interests around this property. A low recycling condition fits better the fast-flowing liquid metal designs that operate at lower temperatures and not to the quasi-static ones, anyway an overall beneficial effect for the plasma to operate in H-mode has been assessed while employing lithium [15]. A compatibility concern is raised due to the reactivity that Li has with water. This requires a protective interlayer made of copper-alloy around the coolant pipe in most designs, but detailed safety analysis is ongoing on this subject.

As far as Sn is concerned, it has a very high latent heat as shown by figure 10, so in principle low evaporation rates are expected. It is also less chemically aggressive than lithium. Nonetheless, the high atomic number makes it harmful if it reaches the core plasma, although until it persists in the divertor region, due to many ionization levels of the atom, it gives great help to reradiate the heat, flattening the heat flux deposition profile [16].

This thesis will consider lithium in its model even though, since the LM debate is still open, extend the analysis to other liquid metals [17] could be also a relevant study and is left for future work.

Symbol (units)	Li	Sn
Atomic no. Z	3	50
Atomic weight	6.94	118.7
Density, $\rho$ (g/mm <sup>3</sup> )	0.512	6.99
Melting point, $T_m$ (°C)	180.5	231.9
Heat of melting, $\Delta H_{melt}$ (J/g)	0.021	0.83
Boiling point, $T_b$ (°C)	1347	2270
Latent heat of vaporization, $\Delta H_{vap}$ (J/g)	1.02	35.15
Dynamic viscosity, $\eta$ (10 <sup>-3</sup> Pa-s) at $T_m$	0.25	1.85
Surface tension, $\sigma$ (Nw/m) at $T_m$	0.4	0.55
Thermal conductivity, $k$ (W/mm-K) at $T_m$	0.045	0.030
Heat capacity, $C_p$ (J/g-K)	4.30	0.250
Volumetric heat capacity, $\rho C_p$ (MJ/m <sup>3</sup> -K)	2.30	1.83
Ionization energy, 1st (10 <sup>6</sup> J/g)	3.61	84.1
Ionization energy, 2nd (10 <sup>6</sup> J/g)	50.6	167.6
Ionization energy, 3rd (10 <sup>6</sup> J/g)	82.0	349.3

*Figure 6: table comparing lithium and tin main properties, adapted from [24].*

### 3.2.3 Liquid metal divertor designs

#### 3.2.3.1 Introduction

Divertor solutions based on liquid metals offer a new spectrum of possible arrangements and properties as plasma facing materials [18]. Here we summarize the main common features shared by the devices exploiting this solution before giving a highlight on each different design.

A liquid metal based PFC is practically free from mechanical damage by neutron and plasma irradiation and it can be renewed in situ with a proper circulation system. Surface deterioration problems are therefore solved. Moreover, it offers other advantages and some drawbacks. The latent heat of vaporization brings a beneficial contribution to the dissipation balance even if it has to be pointed that LM vapor is affected by high redeposition rate due to condensation and backflow to the target (vapor particles are ionized in the plasma sheath in front of the component and undergo prompt deposition on the surface) that mitigate this effect making it almost negligible as heat loss mechanism. Nevertheless, along this cycle, metal vapor particles may undergo collision, in fact the process in which the high energy plasma particle hit the cross section of a low energy metal vapor one produces energy loss by ionizing interaction and bremsstrahlung. This process radiates energy isotropically, flattening the peak load at the divertor target thus resulting in a favorable effect known as vapor shielding. The recirculation of the LM supplied to the divertor also has the potential to allow for a continuous particle exhaust management to some extent.

This configuration has also some drawbacks such as the magnetohydrodynamic effect that may rise instabilities and precarious balance in the LM surface threatening droplet ejection into the SOL. Free flowing liquid has difficulties to adapt to the divertor geometry, the weaker intermolecular force acting in a liquid favors higher quantity of vapor outflow that can potentially contaminate the plasma, a last issue is nested in the D/T retention capabilities of the target that affect recycling and therefore plasma state in the divertor region.

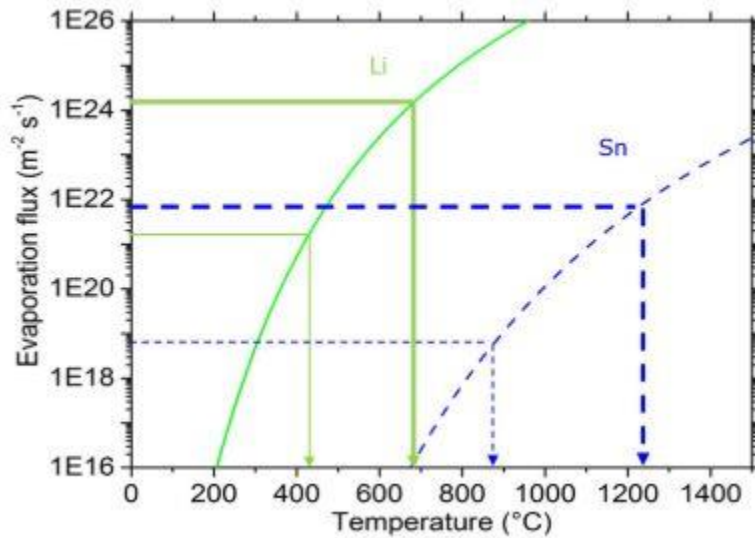


Figure 7: Liquid metals evaporation rates comparison for Li and Sn, limits are for zero redeposition (thin lines) and 99.9% (thick lines), adapted from [14].

### 3.2.3.2 An example of flowing liquid metal divertor: LiMIT

The lithium-metal infused trenches (LiMIT) has been proposed by Ruzic et al [19]. A tile with trenches is used to bind lithium in a trail and thermoelectric magnetohydrodynamic forces (TEMHD) are exploited to passively move lithium from the heated zone and recirculate it. LiMIT belongs to the “fast flowing” category of LM divertor designs, which aim at removing particles and heat loads by mean of a fast-moving LM film. The relatively deep flowing layer can shield inner components and a tritium breeding implementation is possible. On the other hand, the main showstopper are the splashing phenomena and flow instabilities: due to the low LM confinement provided by the trenches, it is more exposed to surface depletion events.

A sample with 20 trenches has been tested at the Solid-Liquid Lithium Divertor Experiment (SLiDE) under a 3MW/m<sup>2</sup> of peak heat flux showing satisfying performances and the potential possibility to remove up to 20 MW/m<sup>2</sup>.

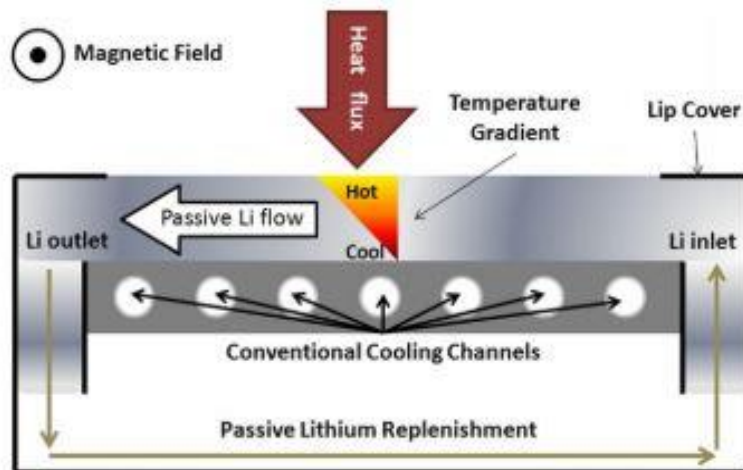


Figure 8: Schematic circuit of the LiMIT design [19].

### 3.2.3.3 The capillary porous structure concept

On the other side with respect to the free flowing concept, there is a quasi-static one that exploits a capillary porous structure to achieve high level of confinement and refill control of the LM. This path was initially pursued by Russian researchers Vertkov, Evtikin and Lyublinsky in the 90's, and growth in interest year by year [20].

The technology offers some attractive feature such as no splashing issues, a flexible choice for the geometry, the capability of the CPS to enhance not only the confinement but also to take care of the replenishment of the LM, always by means of the capillary pressure. It employs small quantities of liquid metal and a concept maturity thanks to the similarities with the heat pipe cooling concept [21] that offers a solid background. Of course even this option, is not free from concern. In fact, due to its quasi-static nature, particle pumping is not feasible as liquid recycling does not reach rates high enough to allow particle control and moreover the high temperature reached by the LM may rise excessive evaporative fluxes exceeding plasma contamination or dilution limits.

Among the latest designs employing a CPS, we can mention the Nagayama proposal of a divertor box [22], the ARLLD model originally developed for the NSTX by Jaworski, Ono and coworkers [23], or the one under study at KTM by Lyublinsky et al. [24].

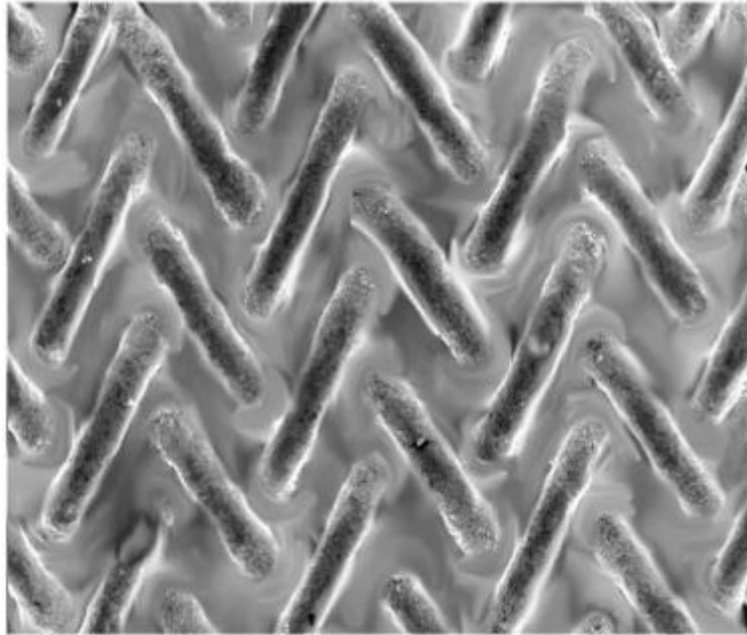


*Figure 9: Magnification of the mesh of the capillary porous structure wetted by liquid lithium [24].*

#### **3.2.3.4 Vapor box**

Nagayama's idea is to implement two chambers in proximity of a liquid metal covered divertor. The chamber that contains the LM target is the outer one and is called the Evaporation Chamber (EC) since most of the evaporation take place there, instead, the first chamber to be entered by the SOL plasma is the Differential Chamber (DC), that aim to realize differential pumping between the plasma chamber and the Evaporation Chamber.

Plasma strike point can be a pool of liquid metal since splashing phenomena issues are mitigated by the chamber closure, or –more realistically- a liquid metal filled CPS. The design intends to exploit liquid metal latent heat and vapor shield at its finest, decoupling the LM dedicated region from the main plasma. Due to the two boxes high evaporative fluxes can be achieved without excessive plasma pollution, or dilution risk since lithium is the metal considered here; the lithium vapor is favored to condense also on the wall of the chambers that are water cooled and covered with a textured surface to help spreading condensation

surface and condensed lithium recirculating process. To deal with non-condensable gases, both chambers are evacuated by vacuum pumps. The vapor shielding coupled with the condensation on the walls mitigates the huge peak loads on the strike point. The openings on the chamber entrances have to be as narrow as possible, but at the same time letting room for eventual fluctuation of the magnetic field and therefore of the hot plasma. A better insight of the plasma side mechanics inside the boxes is fundamental to validate the proposal and is nowadays under investigation. Moreover, due to the unconventional divertor structure, placing problem has to be accurately envisioned to adopt a geometry that fits with the coils structure underneath [25].

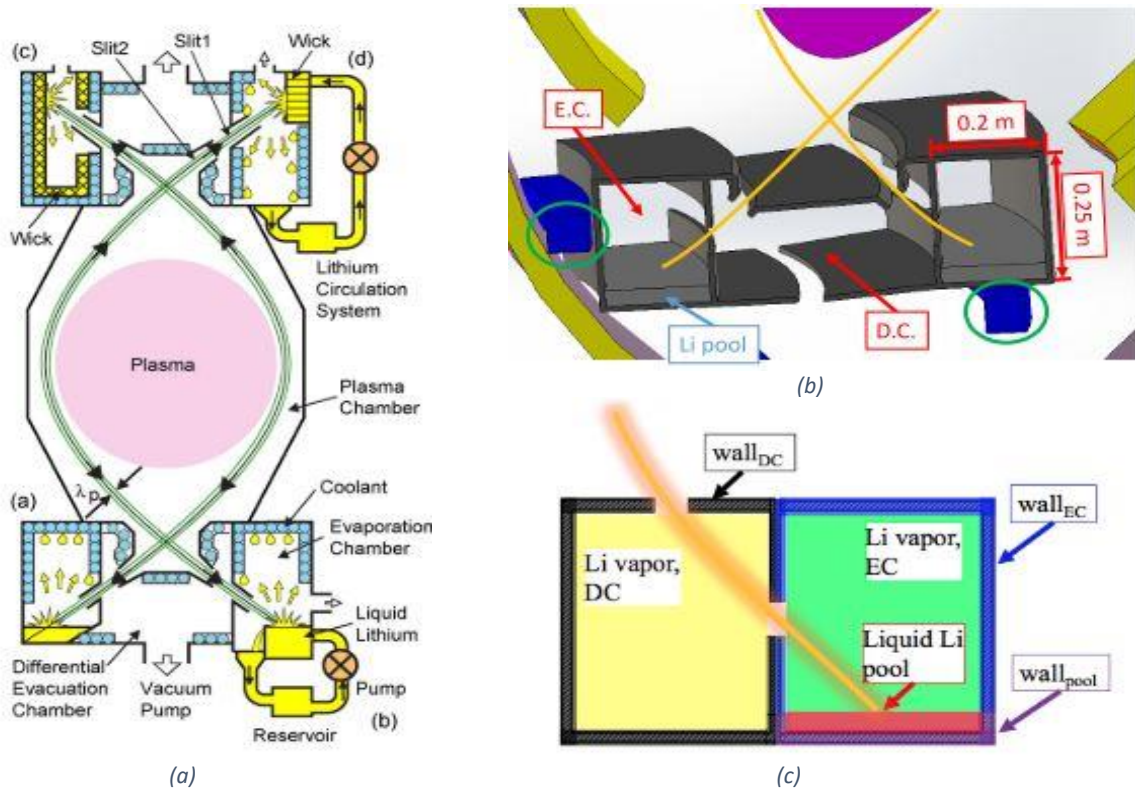


Figure 10: schematic view of Nagayama's designs (a), casing of the box in the plasma chamber (b) and (c) example of the model of the chambers for simulating purpose adapted from [22], [25].

## 4 Aim of the work

The DTT main objectives are to find a safe and robust power handling solution for DEMO and maintain the plasma parameters as close as possible to the values foreseen for DEMO [6]. It is also required, among the technological features, to have a flexible divertor region (in order to test as many different solutions as possible), a moldable magnetic configuration (to test alternative shapes), and the possibility to test liquid metals solutions. DTT and DEMO main parameters are summed up in figure 11 as well as the ones of several other tokamak machines.

	JET	AUG	EAST	DIII-D	ITER	DEMO	JT-60SA	WEST	TCV	ADX	DTT
R (m)	2.98	1.65	1.7	1.67	6.2	8.77	3.0	2.5	0.88	0.73	2.15
a(m)	0.94	0.5	0.4	0.67	2.0	2.83	1.2	0.5	0.24	0.2	0.70
I <sub>p</sub> (MA)	3.5	1.6	1.4	2.0	15	20	5.5	1	0.45	1.5	6.0
B <sub>T</sub> (T)	3.2	2.4	3.4	2.1	5.3	5.8	2.3	3.7	1.45	6.5	6.0
V <sub>0</sub> (m <sup>3</sup> )	82	13	10	19	853	2218	141	15	1.85	0.9	33
<n> (10 <sup>20</sup> m <sup>-3</sup> )	0.9	0.9	1.0	0.85	1.0	0.9	0.9	0.8	1.2	4.5	1.72
<n>/n <sub>c</sub>	0.7	0.5	0.4	0.65	0.85	1.1	0.8	0.7	0.5	0.4	0.45
P <sub>tot</sub> (MW)	30	25	30	27	120	450	41	16	4.5	14	45
τ <sub>E</sub> (s) (H <sub>98</sub> = 1)	0.49	0.07	0.07	0.11	3.6	3.4	0.62	0.05	0.027	0.05	0.47
<T> (KeV)	3.3	2.5	3.3	2.8	8.5	12.6	3.4	2	0.8	1.7	6.2
β <sub>N</sub>	1.8	2.4	2.2	2.9	1.6	2.1	2.4	2	2.7	2.2	1.5
ν* (10 <sup>-2</sup> )	8.6	8.4	7.4	4.0	2.3	1.3	4.1	35	65	13.1	2.4
ρ* (10 <sup>-3</sup> )	4.0	8.5	8.5	7.2	2.0	1.6	4.5	5.0	17	7.7	3.7
T <sub>ped</sub> (KeV)	1.7	1.3	1.7	1.4	4.3	7.0	1.7	0.5	400	1.3	3.1
n <sub>ped</sub> (10 <sup>20</sup> m <sup>-3</sup> )	0.7	0.7	0.9	0.7	0.8	0.7	0.7	0.5	0.9	3.8	1.4
ν <sup>*</sup> <sub>ped</sub> (10 <sup>-2</sup> )	22.6	22	21	10	6.2	2.8	11	92	170	35	6.3
ELMs En. (MJ)	0.45	0.06	0.07	0.13	24	140	1.1	0.2	0.03	0.02	1.2
L-H Pow. (MW)	9.5-12	3-4	3.5-4.5	3.0-4.0	60-100	120-200	10-12	4-6	0.6-0.8	4-6	16-22
P <sub>sep/R</sub> (MW/m)	7	11	12	11	14	17	9.5	4	3.4	13	15
λ <sub>int</sub> (mm)	3.2	3.7	2.6	3.6	2.2	2.2	3.7	3	5.5	1.7	1.7
P <sub>div</sub> (MW/m <sup>2</sup> ) (no Rad)	28	44	62	45	55	84	24	25	7.3	110	54
P <sub>div</sub> (MW/m <sup>2</sup> ) (70% Rad)	8.6	13	19	13	27	42	7.4	7.5	2.2	33	27
q// ≈ P <sub>tot</sub> /R (MW T/m)	32	44	60	40	100	290	22	23	5	125	125
Pulse Length (s)	≈ 20	≈ 6	??	≈ 6	400	7000	100	1000	5	3	100

Figure 11: table adapted from [3], summarizing the relevant parameters of the main tokamak designs.

The objective of the thesis is to determine the requirements for the LM confinement and circulation in the CPS, based on the balance between the various forces present in the system. This is done also by relying on a simplified 2D thermoelectric model for the most stressed divertor zone.

The case of study refers therefore to a section of the whole divertor component due to the small dimension of the interested zone (~cm). The domain is made up of the cps structure and the substrate, up to the interface with the coolant. A starting case is taken with geometry and shape adapted from [26] and discussed in section 6. This can be transposed with a

foreseen little difference in the final results to other devices employing the same technology and principles.

The results of this work should therefore answer the following questions: is the liquid metal successfully confined into the CPS without droplet ejection and excessive evaporation into the SOL for DEMO-relevant conditions? Is the capillary pumping sufficient to recover the evaporation rate of liquid metal leaving the CPS surface? Do the properties of the materials employed stay within the working thresholds during steady state operating regime?

## 5 Problem definition and preliminary calculations

### 5.1 Pressure balance

The advantages of a CPS based divertor have been summarized in section 3.2.3.3. The assessment of the limits of the technology is still under development and this work aims to progress in this direction, with a focus mainly on the component point of view, leaving plasma conditions aside.

A well suited CPS should guarantee the self-recovery or replenishment of the lattice after material loss through erosion and evaporation mechanism, the homogeneous distribution of the LM inside the wick, the confinement of the lithium inside the target plate and drive a circulation within the divertor pit hydraulically connecting evaporating and condensing surfaces.

Before approaching the assessment, is essential to evidence the phenomenology affecting the liquid metal equilibrium inside the CPS. The forces acting as pressure contributions on the generic liquid element and therefore responsible for its motion are listed below under the form of an inequality adapted from [27]. If satisfied, this inequality ensures the dominance of the capillary pressure related term  $P_c$  over the cumulative effort of all the other pressure contributions.

Verifying this inequality (2) is crucial to benefit from the features offered by a capillary force dominated regime that will be carefully treated in the following sections as long as an insight of each term of (2) will be given.

$$P_c \geq \Delta P_t + \Delta P_f + \Delta P_m + \Delta P_h + P_o + P_p \quad (2)$$

$P_c$  refers to the capillary force acting on the meniscus formed at liquid-vapor interface,  $\Delta P_t$  represent the pressure drop at the liquid-vapor phase transition,  $\Delta P_f$  embed the hydrodynamic pressure difference due to friction loss in the lattice and the one related to Magnetohydrodynamic (MHD) brake,  $\Delta P_m$  refers to magnetic field interaction with Thermoelectric (TE) currents,  $\Delta P_h$  refers to the hydrostatic pressure drop and  $P_p$  and  $P_o$  are the pressure of the plasma in front of the CPS surface and the one in the supply system

respectively. In the following, further details concerning each pressure contribution are presented.

### 5.1.1 Capillary pressure

The capillary pressure is derived from the interaction of forces between a fluid and a solid wall and can restrain or promote fluid transport.

This force exerted on the liquid-solid interface is propagated on the meniscus thanks to the surface tension of the liquid. It is in fact defined as a function of the surface tension  $\sigma$  and the radius of the meniscus [28]:

$$P_c = \sigma \left( \frac{1}{R_1} + \frac{1}{R_2} \right) \quad (3)$$

Where

- $\sigma$  is the liquid surface tension in N/m;
- $R_1$  and  $R_2$  are the principal radii of the meniscus that can show different concavities dependently with the tube shape.

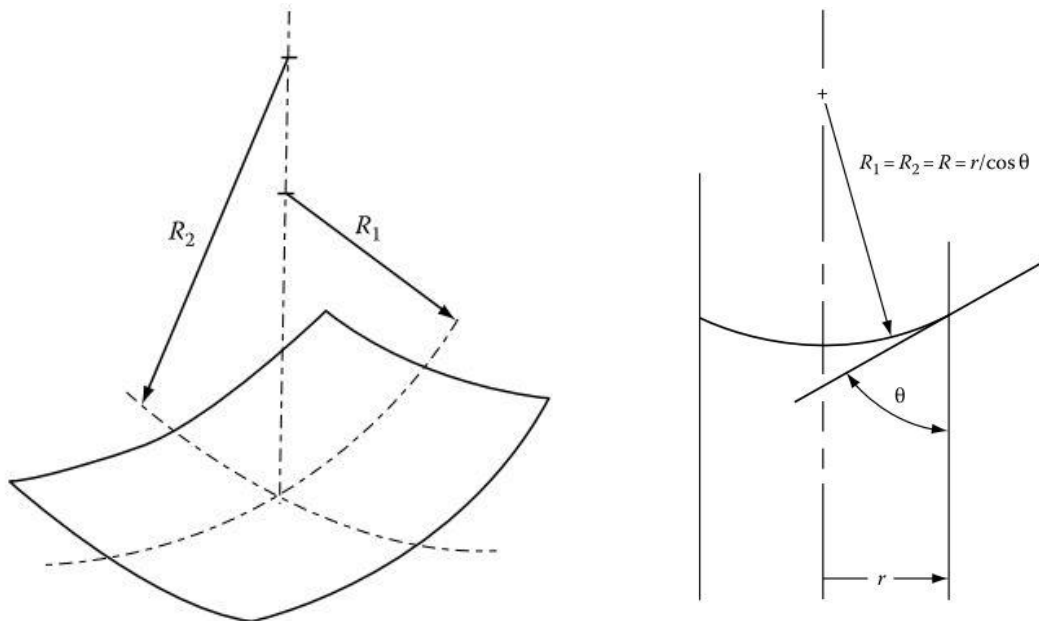


Figure 12: left figure, general meniscus radii, right one meniscus radius in a cylindrical capillary tube.

The radius of the meniscus is linked to the dimension of the capillary tube by the wettability between the solid liquid pair taken into consideration. The wetting angle reflects the capability of the liquid to reject or spread on the contact surface; in case of a cylindrical capillary tube the previous relation reduces to:

$$P_c = \frac{2\sigma \cos\theta}{r} \quad (4)$$

Where

- $\theta$  is the wetting angle;
- $r$  is the radius of the cylindrical pore;

It is remarkable to state that according to the orientation of the meniscus cavity, the capillary pressure exerts a force pointing upward in the porous channel (in case of under-pressure helping the replenishment of the CPS), or a force pointing downward (in case of over-pressure inside the CPS). It is important to recall that the liquid-vapor interface on the top of the CPS adapts its surface concavity to counterbalance the eventual under/overpressure present in the system; so the  $P_c$  term refers to the maximum capillary pressure available for pumping or confining the liquid trapped in the CPS.

### **5.1.2 Pressure drop at liquid-vapor phase transition**

This contribution is often neglected in the heat pipes formulation due to the low magnitudes it has with regards to other pressures involved, but it might show a not negligible value when the cases refer to high heat loads or microscopic porosities, which are both present in the system considered [29]. Available literature is not univocal on determining the formulation for this term. For the purpose of this thesis, we shall employ the most updated formulation cited.

According to the paper by I. E. Lyublinski and coworkers [30] the equation state as follow:

$$\Delta P_t = \frac{1}{2} P_e \quad (5)$$

Where  $P_e$  is the vapor pressure of the liquid evaluated at the interface temperature.

### 5.1.3 Hydrodynamic and hydrostatic pressure drop

The hydrodynamic pressure drop refers to the resistance encountered by the LM flow due to viscous forces. For this specific case, where the motion take place inside a porous medium, in laminar regime such condition is taken in account by the Darcy formulation which regulates the pressure drop for fluid in motion inside porous medium and sediments. This pressure drop is expressed as follows:

$$\Delta P_{f,d} = \frac{\mu \dot{m}'' L}{\rho k_o} \quad (6)$$

Where

- $\mu$  refers to the dynamic viscosity of the liquid in Pa·s;
- $\dot{m}''$  is the specific mass flow rate in kg/s/m<sup>2</sup>;
- $L$  is the length of the path travelled by the liquid from supply point to the CPS surface in m;
- $\rho$  is the liquid density in kg/m<sup>3</sup>;
- $k_o$  is the porous medium permeability in m<sup>2</sup>;

The hydrostatic pressure drop takes in account the pressure loss due to potential body force acting on the fluid, in this case the gravitational one, and is evaluated by the well know term of the Bernoulli equation:

$$\Delta P_h = \rho g h \quad (7)$$

Where

- $g$  is the gravity force in  $\text{m/s}^2$ ;
- $h$  is the height of the liquid column;

### 5.1.4 Plasma pressure and pressure in supply system

The supply pressure  $P_0$  refers to the pumping pressure in the supply system and can be an input parameter of the inequality (2). The choice of this parameter can follow an accurate quantitative study of other pressures involved in the circulation system and for sake of simplicity is neglected in this framework. This contribution, if present, will help the replenishment of the CPS, therefore this assumption will be a conservative hypothesis from the refilling point of view. Instead, plasma pressure is briefly reported below, its distribution is shown in the following graph adapted from [31]. The graph is a result of simulations of the SOL plasma in DEMO relevant conditions.

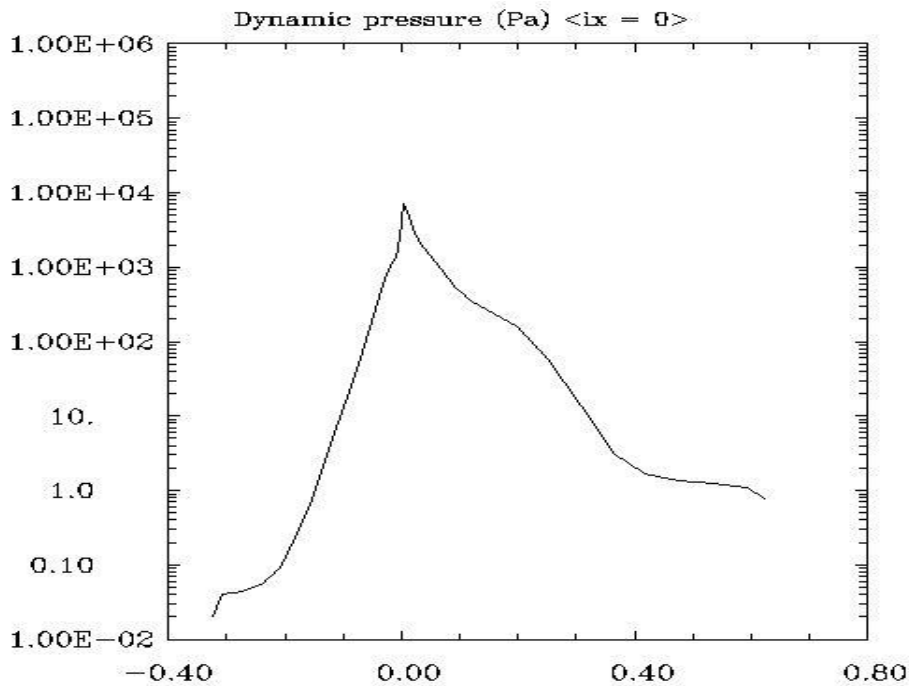


*Figure 13: Plasma pressure profile above divertor plate in DEMO relevant conditions, as a function of distance from the separatrix, for the outboard divertor plate.*

### 5.1.5 Pressure drop due to magnetic field interaction

This kind of term is made of two contributions: the pressure resistance due to MHD and a TEMHD related term that needs a more in depth treatment to be fully understood.

MHD refers to the capability of a conductive fluid in motion to interact with a magnetic field when crossing it. The free charges dispersed in the metal once in motion interact with the magnetic field experiencing the Lorentz force that deviates their path generating a current normal to the fluid velocity. Moreover, the magnetic field also interacts with the new born current and again the cross product between the electric current and the magnetic field results in a force with the same direction of the initial fluid velocity but pointing the opposite way as figure 14 sketch out. This effect brakes the fluid motion and raises the overall pressure drop per unit path length.

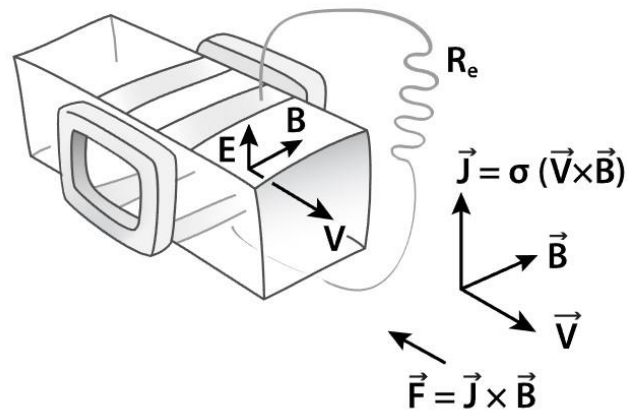


Figure 14: MHD force formation [adapted from Wikipedia].

To relate such magnetic force to the viscous one a dimensionless number called the Hartmann number is used which is determined by the ratio of the two:

$$Ha = Bd_h \sqrt{\frac{\sigma_e}{\mu}} \quad (8)$$

Where

- $B$  is the magnetic field in T;
- $d_h$  is the characteristic length scale, (the pore size in this case) in m;
- $\sigma_e$  is the electric conductivity in S/m;

To put the magnitudes of the involved phenomena in the right perspective, for this case of study, we refer to L. Bühler results [32] to estimate MHD related pressure drop in porous medium as a function of the Hartmann number.

As far as the TEMHD is concerned, it is a phenomenon that has come to the attention in the last decade in the fusion community. Indeed, as the liquid metal proposals started gaining increased attention, it has been thought to exploit this effect for moving LM in the divertor. This effect couples two well-known effects: the thermo-electric generation and the aforementioned magnetic interaction with electric currents flowing in a fluid. For a complete treatment of the TEMHD we refer to [33], but provide here a glance of the thermo-electric effect in question. The effect is introduced in an equation as follow:

$$\vec{j} = \sigma_e (-\nabla\phi + \vec{v} \times \vec{B} - S\nabla T) \quad (9)$$

Where

- $\vec{j}$  is the electric current density in A/m<sup>2</sup>;
- $\phi$  is the electric potential in V;
- $\vec{v}$  is the velocity of the medium in m/s;
- $S$  is the Seebeck coefficient or absolute thermoelectric power in V/K;
- $T$  is the temperature in K;

Each of those terms has the capability to induce a current and therefore has to be taken in account while performing a TEMHD analysis. The thermo-electric term is the last one and depends on the Seebeck coefficient and on the temperature gradient;  $S$ , the absolute thermoelectric power measures the capability of a material to build up an electromotive force  $E_{mf}$  in response to a temperature difference across that material, and is the basic working principle of thermocouples.

It is worth to state that if two different materials with different Seebeck coefficient are connected by their extremities each of which is kept at a different temperature as in figure 15, a current loop will arise as consequence of the interaction of the two different electric potential generated in the respective materials.

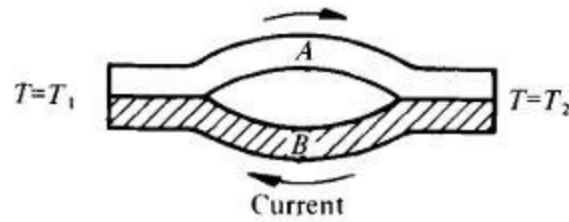


*Figure 15: Thermo-electric current formation, in this case materials A and B have different Seebeck coefficients [33].*

If the setup cited above is contextualized in our divertor case, the liquid metal and the substrate holding the CPS coupled with the broad thermal gradients experienced by the component offer the ideal environment for such an effect to rise in a continuum domain. It might be significant therefore to perform an adequate estimation of the current flowing into the liquid metal produced by this effect and its interaction with the magnetic field.

## 6 The model

### 6.1 Preliminary calculations

A preliminary simplified 0D model is made in order to have a grasp of the orders of magnitude of phenomena mentioned above and of the needed hypothesis for a more detailed 2D simulation. An a posteriori verification will tell if this model, is suitable to roughly predict the expected ranges of operability of the component in terms of temperature, lithium flowrate and related pressures.

Below, the assumptions and the rationale of the model are listed. It is supposed to employ data available in the literature, inheriting the main useful parameters like material composition, thickness, CPS porosity and is then intended to provide a benchmark case used to perform a parametric analysis with conservative hypothesis where needed.

The model considers a tungsten CPS filled with liquid Lithium. Tungsten is a well-known material adopted in fusion PFCs, performing well at elevate temperatures under harsh environment with high particles and heat fluxes. Other relevant possibilities can be molybdenum or vanadium alloys. Lithium is employed for reasons cited in section 3.2.2, and it is compatible with tungsten for temperatures up to 1500 °C [34].

In the following table assumed data are summarized:

*Table 1: Data assumed for the simulation.*

Quantity	Symbol	Value	Unit	Motivation for the choice
Specific heat load	$Q_{div}''$	6	MW/m <sup>2</sup>	Close to the average heat load impinging the divertor zone considered for 2D model
CPS pore size	$d_h$	30	μm	Metal felt CPS with pore size according to [26]
CPS-Substrate interface temperature	$T_{in}$	850	K	A posteriori verified with a refined thermo-electric 2D model

CPS wick height	h	2	mm	Mid-range value according to literature specimen [14]
Liquid path from supply point to main evaporative spot	$L_{sc}$	2.5	cm	Hypothetical monoblock poloidal half-width, replenishment from both sides is foreseen.
CPS porosity	$\varepsilon_p$	0.4	-	According to [26]
CPS wire diameter	$d_w$	50	$\mu\text{m}$	According to [26]
Toroidal magnetic field in outer divertor region	B	5	T	In range with the one estimated for DEMO divertor condition
Wetting angle between liquid Li and W	$\Theta$	0	deg	Perfect wettability achievable according to [34]
Permeability	$k_o$	$1.39 \cdot 10^{-11}$	$\text{m}^2$	Metal felt wicks correlation from [35]
Redeposition	R	0.90	-	Conservative rate from [36]

The scheme of the simulation performed with MATLAB is based on an energy balance in the CPS of the form:

$$Q''_{div} = Q''_{ev} + Q''_{cond} \quad (10)$$

Where  $Q''_{ev}$  and  $Q''_{cond}$  are the specific heat load dissipated by evaporation and conduction respectively, (thermal radiation contribution from the CPS surface is still of negligible magnitude and can be ignored).

The aim of this balance is to evaluate, through an iterative solution, the CPS surface temperature that verifies it, in such a way that  $Q''_{ev}$  can be estimated and therefore also the

specific flowrate of Lithium needed to replenish the CPS. The surface temperature helps to estimate the liquid vapor phase transition pressure drop by mean of the saturation pressure, and the supply flowrate is fundamental to calculate the pressure loss due to viscous friction and MHD. In this way, this simplified model can be employed to provide estimates of the various term of the pressure balance.

To explicitly formulate the evaporative term, equation (11) from Safarian paper [37] is employed to evaluate the particles flowrate and then properly convert it to a heat flux through Li latent heat of evaporation. The regime of “weak evaporation” is assumed. The condensation term is neglected since Li will likely condensate on nearby surfaces. This approach leads to a conservative estimation of the needed flowrate increasing the pressure drop. Evaporated particles undergo prompt redeposition as they can be ionized in the immediate proximity of the target. A conservative estimate of the prompt redeposition coefficient  $\beta=0.90$ .

$$Q''_{ev} = \sqrt{Li_m} \eta \beta H_{fg} \frac{P_{sat}(T_i)}{\sqrt{2\pi K_b T_i}} \quad (11)$$

Where:

- $Li_m$  is the Li atom mass in kg;
- $\eta$  is a dimensionless factor estimated from [37] and equal to 1.66;
- $\beta$  is the prompt redeposition coefficient;
- $H_{fg}$  is the evaporation latent heat of Li in J/kg;
- $P_{sat}(T_i)$  is the Li saturation pressure at temperature  $T_i$  in Pa;
- $K_b$  is the Boltzmann constant in J/K;
- $T_i$  is the temperature of the i-th surface in K;

The conductive term through the CPS come from classical Fourier law:

$$Q''_{cond} = \frac{K_{cps}}{h} (T_i - T_{in}) \quad (12)$$

Where  $K_{cps}$  is the predicted thermal conductivity of the CPS in W/m/K and is calculated according to [38] by mean of the law of mixtures,  $K_{cps} = K_{Li} \varepsilon_p + K_W(1 - \varepsilon_p)$ , i.e. the different thermal conductivities of Li and W are weighted on the porosity of the CPS and evaluated at an average temperature in-between the maximum surface temperature expected and the interface one.

The solution of this balance is achieved by solving a nonlinear set of equation by means of the MATLAB function `fsolve`. The resulting surface temperature is  $T_i$  of 976 K to which correspond an evaporative flowrate  $\dot{m}''_{ev}$  of  $\sim 0.0035$  kg/m<sup>2</sup>/s.

In order to compensate for this mass loss, an amount of liquid Li mass flow by the cps edges in the toroidal direction, with an expected intake specific flowrate of  $\dot{m}'' = 0.0433$  kg/m<sup>2</sup>/s. This correspond to a slow replenishment velocity of 0.00009 m/s, which a posteriori confirms the assumption of a quasi-static regime.

Most of the pressure contributions can now be roughly framed with the order of magnitude expected in the CPS application except for the one related to thermo-electric effect. This is due to the fact that the dependence on the temperature gradient is a local feature strictly related to the poloidal shape of the power load in the divertor hot point zone. Whereas this 0D model only employs an average heat flux, leading to an average temperature, with the impossibility of evaluating temperature gradients. Moreover, it would not be satisfactory to employ temperature profiles from the literature. Therefore, a 2D model to figure out the temperature and mostly the electric current density distribution is essential to this purpose and is presented in the following section.

## 6.1 2D thermo-electric model

A finite element method is here employed to study a poloidal section taken in the toroidal midpoint of the ideal monoblock in exam, see figure (16) [39]. The open source code FreeFem++ is used to solve the 2D model. Two reason lay behind this choice: the toroidal symmetry of the power load, and the fact that the middle of the monoblock is the closest to the coolant channel and so experience the highest temperature gradients.

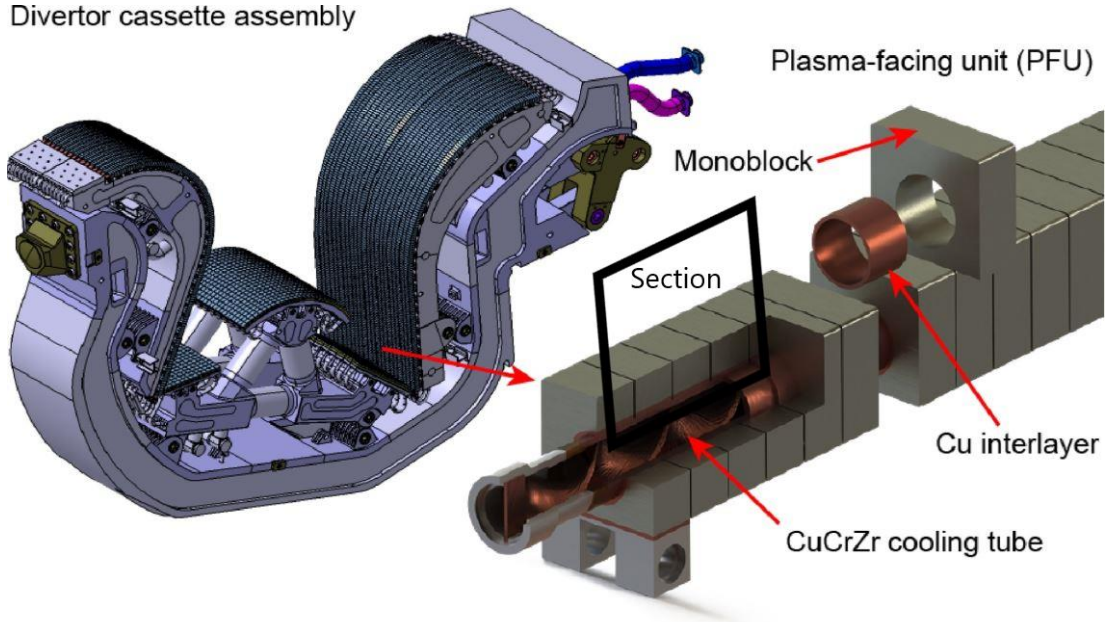


*Figure 16: Divertor cassette and PFU section of interest, adapted from [39].*

As the design of CPS targets based on the CPS concept is still evolving, we shall assume in this thesis a representative configuration of the LM divertor, which is however not to be considered the final one.

The characteristics of the monoblock layers underneath the CPS are inherited by [40], water is used as coolant, flowing in a CuCrZr pipe of thickness 1.5 mm and a Cu interlayer of 1 mm connects it to a 6 mm tungsten armor substrate that holds the CPS in place. The poloidal length is taken equal to 5 cm to reach a region where poloidal gradient is exhausted so adiabatic condition is realistic.

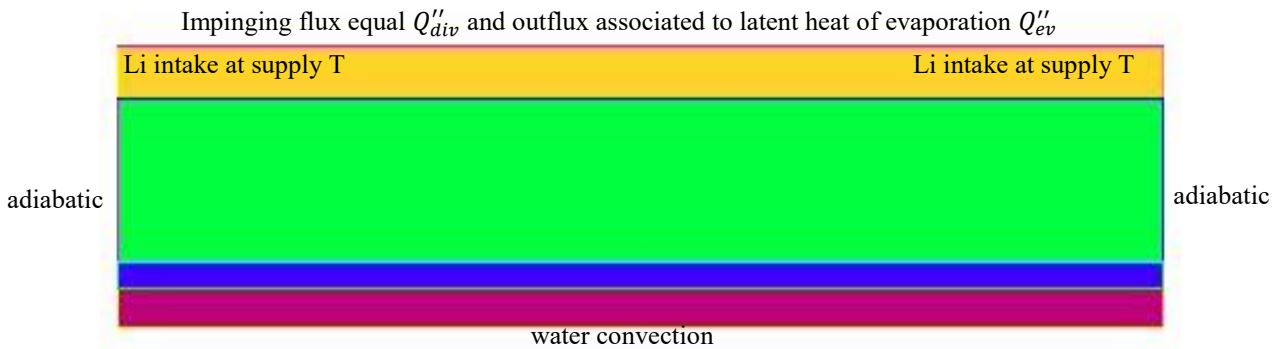


*Figure 17: poloidal section of the reference monoblock with boundary condition indicated.*

### 6.1.1 Thermal model

Thermal model consideration:

- The thermal conductivities are evaluated as a function of the temperature and weighted over the porosity in the CPS region;
- The heat transfer mechanism considered through the CPS is only conduction due to the quasi-static regime of the Li (i.e. advection is neglected);
- Steady state problem, transient behaviors are left for future study;
- Thermal and electric state are solved in a decoupled manner; Joule effect power generation, which would be coupling the two fields is assumed negligible;
- For 0D calculation, an average heat flux of  $6 \text{ MW/m}^2$  was employed, as stated in table 1. For a 2D calculation it is instead needed to consider the actual poloidal shape of the power deposition.
- The Power load density shape here assumed is based on estimation by Dr. P. Rindt [36] and quantitatively is adapted from [41] equal to a constant pedestal away from the strike point  $Q''_{ped} = 5 \text{ MW/m}^2$  with an additional exponential load with a maximum  $\sim 21 \text{ MW/m}^2$  -conservatively simulating slow transient event like plasma reattachment- impinging the center of the CPS and decaying away the peak point towards increasing x.

$$Q''_{div} = Q''_{ped} + Q''_{peak} \frac{1}{0.005} e^{\left(-\frac{(x-\frac{L}{2})}{0.005}\right)} * \left(x \geq \frac{L}{2} + 0.001\right) \quad (13)$$

Where:

- $Q''_{peak} = 100 \text{ kW/m}^2$ ;
- $L$  is the CPS poloidal length in m;

Therefore, the reference heat load impinging the CPS surface is represented below:

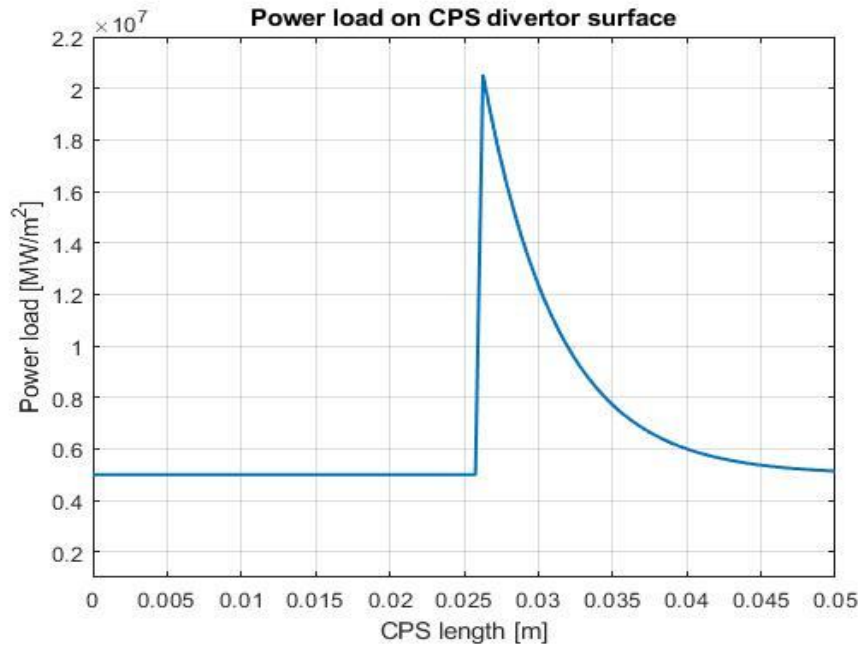


Figure 18: Power load  $Q''_{div}$  on CPS divertor surface.

The heat load tries to mimic the expected one under real condition, it undergoes a steep exponential decrease to few  $\text{MW/m}^2$  in the range of a couple of centimeter due to the narrow power width, moreover the “pedestal” tries to emulate the radiative contribution that is equally spread over the surface and it is the only one that can get to the private plasma region.

It has to pointed out that the actual power entering the SOL and aiming the divertor as figure 11 shows for the  $P_{div}$  datum would lead to a higher heat load than the

simulated one. It is in fact foreseen that most of this power will be mitigated by means of impurity seeding in the SOL. Gaseous mixture like Argon and Xenon can reradiate up to 64% of the incoming power [42]. Moreover, Lithium vapor shielding and non-coronal radiation [43] help in the same manner flattening the peak. The evaluation here performed neglects this feedback associated to the effect of evaporated Li on plasma, although this is currently being investigated[44].

- Convection heat transfer coefficient between CuCrZr pipe and water coolant is evaluated according to the correlation proposed by [40] and reach tens of thousands of  $\text{W/m}^2/\text{K}$ ;
- Coolant temperature profile, along the poloidal direction, is estimated following the linear best-fit trend obtained by solving the same problem on the monoblock but on adjacent poloidal sections keeping track of the energy intake of the coolant and therefore its temperature increase section by section; subcooled water at inlet temperature of  $\sim 84^\circ\text{C}$  will reach an outlet one of  $\sim 90^\circ\text{C}$ ;
- Boundary condition are the ones summarized in figure 17;
- The energy balance introduced in equation (10) is applied on CPS Li surface until convergence of the 2D temperature field;
- A relaxation factor is adopted for the evaporative flowrate to approach solution in a smoother way avoiding broad fluctuation in the early iterations
- A Li supply is envisioned entering the edges of the CPS at the supposed Li pool thermodynamic state ( $\sim 500\text{K}$ ), to replace the evaporated one;

Thermal solution is presented in figure 19. It shows a maximum Li temperature near  $\sim 900^\circ\text{C}$  rapidly decreasing away from the central strike point following the power load shape to more bearable values  $500\text{-}700^\circ\text{C}$  in terms of related Li mass evaporative flux, an overall specific Li evaporation rate of  $7.7 \text{ g/m}^2/\text{s}$  thus leading to a net particles outflux  $N_{\text{out}} = 6.6 \cdot 10^{23} \text{ atom/m}^2/\text{s}$ , it locally exceed the tolerable limit as figure 6 shows but since this extreme condition is reached during slow transient such impurity input is not a steady condition for the SOL. As mentioned above, a SOL plasma model aiming to assess evaporation limits during slow transient is a topic that need to be addressed in a future study. The temperature



### 6.1.2 Electric potential model

The equation for the current density state as equation (14) reports:

$$\vec{j} = \sigma_e(-\nabla\phi + \vec{v} \times \vec{B} - S\nabla T) \quad (14)$$

The current density must satisfy the zero divergence condition,  $\nabla \cdot \vec{j} = 0$ . The quasi-static condition causes the  $\vec{v} \times \vec{B}$  term to drop, thus the equation becomes:

$$0 = \nabla \cdot (-\nabla\phi - S\nabla T) \quad (15)$$

And if we group the potential  $\phi$  and the thermo-electric one that can be identified just by  $ST$  being the Seebeck no spatial dependence, a global potential  $U$  can be defined by summing both contributions,  $U = \phi + ST$ .

A final and simplified version of equation (15) becomes:

$$\nabla^2 U = 0 \quad (16)$$

Therefore, the solution of the problem is reduced to a Laplace equation for the potential  $U$ ; being the temperature profile known a priori everywhere the boundary conditions can be either posed on  $\phi$  or directly on  $U$ . To simplify the problem, and being the current density needed only the one flowing in the CPS, the domain is reduced to the CPS and the closest tungsten substrate with the boundary conditions on the borders presented in figure 21:

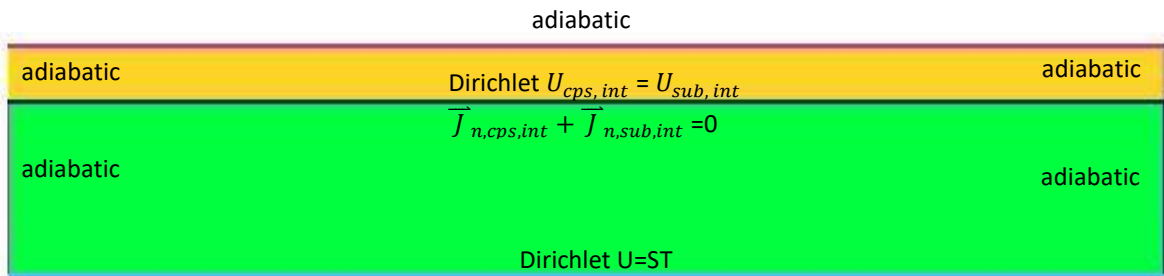


Figure 21: Electric domain and boundary condition.

The adiabatic condition on the CPS surface is taken as a conservative choice since it will force current to circulate along the poloidal direction the only one affecting the TEMHD pressure under study. The sides are assumed to be adiabatic as well since they are considered to be far enough not to significantly affect the solution with this choice. As far as the bottom one is concerned, it has a Dirichlet condition coincident with the thermoelectric potential as suggested by [45].

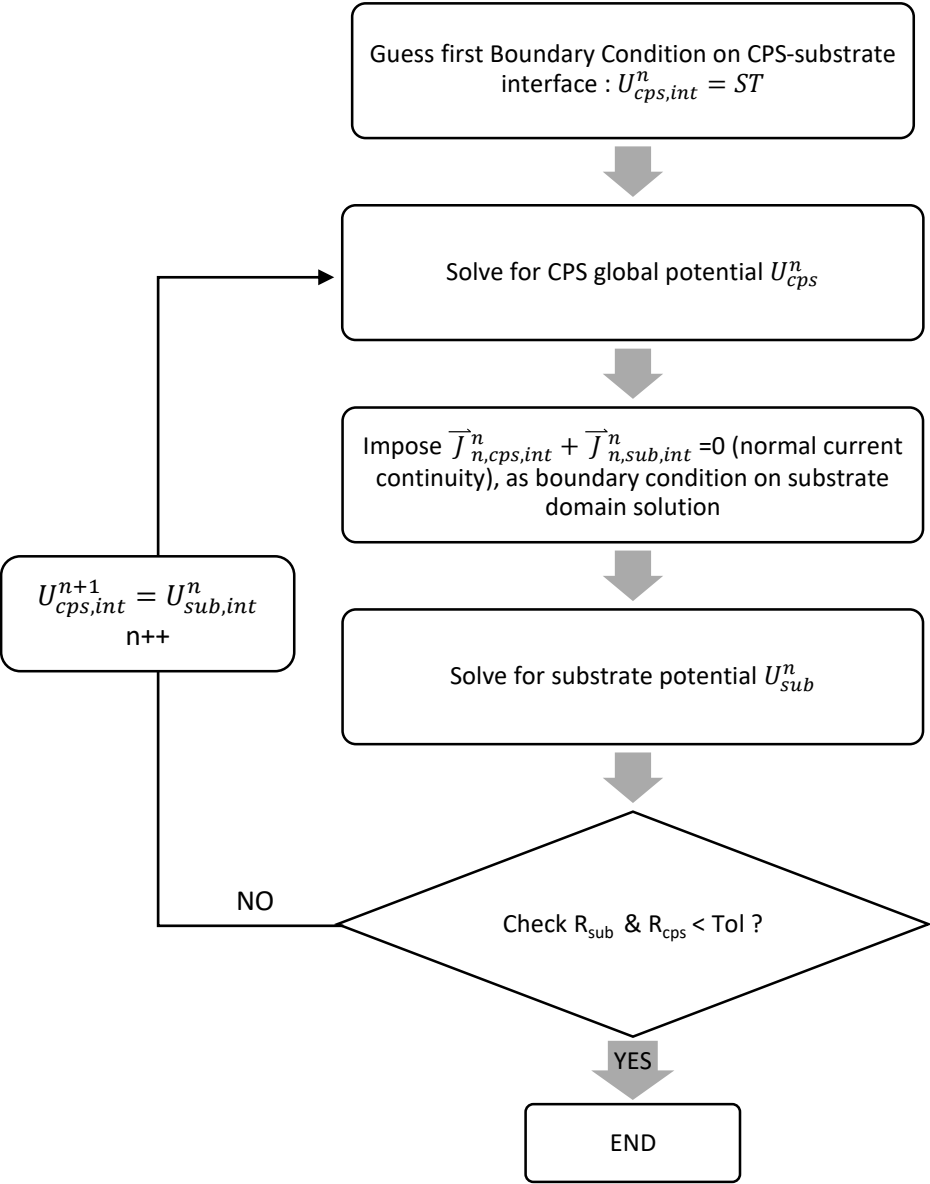


Figure 22: Potential solution scheme.

The figure 22 shows the iterative process for the solution of the potential, where the domains are solved separately and coupled by the interface boundary condition.

Where:

- $R_{cps}$  and  $R_{sub}$  are the relative errors of two successive iteration expressed as
 
$$R = \frac{|U^n - U^{n-1}|}{U^n};$$
- $U_{cps,int}$  and  $U_{sub,int}$  are the potential of the CPS and substrate domain on the interface;
- $\vec{J}_{n,cps,int}$  and  $\vec{J}_{n,sub,int}$  are the interface normal current densities in the CPS and substrate domain respectively;
- The superscript ‘n’ identifies the iteration number.

#### 6.1.2.1 Electric model benchmark and TEMHD contribution

The electric model implementation is at first verified by solving a problem found in literature [45]. The author Fan calculate the electric potential and the current generated between two different phases -with 2 different Seebeck coefficients- during the solidification of an alloy; in particular, he analyzed a solid grain immersed in a liquid phase crossed by a constant temperature gradient, oriented according to the white arrow in figure 23 (a). The principle is the same used by Kaldre [46] in a fusion related case of a CPS filled with liquid lithium under inhomogeneous heat load.

The two figures below compare the results obtained by FreeFem++ code with the ones published in the article by Fan.

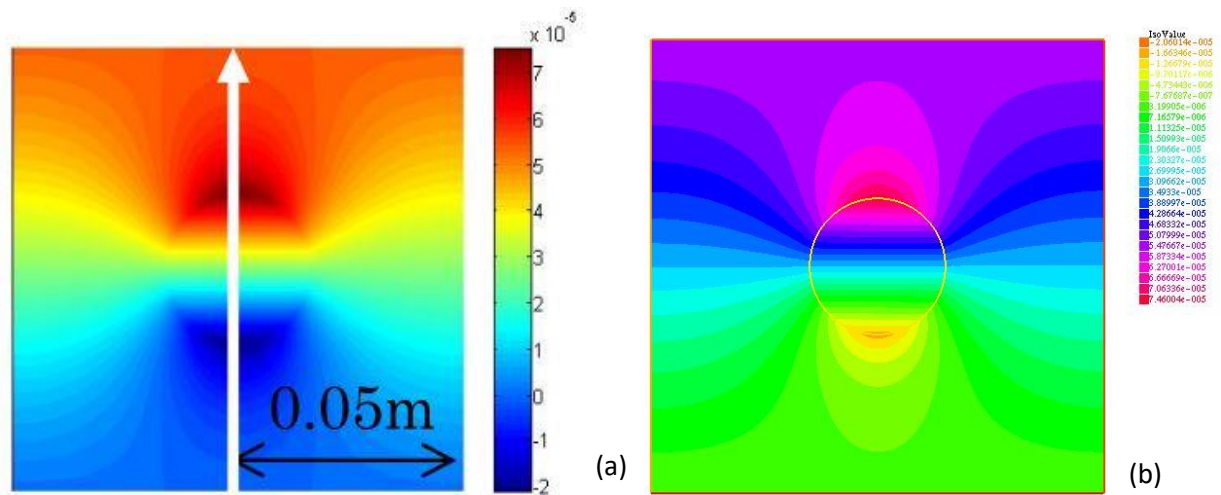


Figure 23: Fan model (a) and coded one (b) electric potential comparison [V].

The distribution of the electric potential correspond both in shape and magnitude, confirming the good implementation of the model.

Here the solution of the currents circulation on the case of study is presented (figure 24).

It is worth to state that CPS and substrate resistivity is assumed equal to the lithium and tungsten one respectively, evaluated according to a temperature correlation [47], [48].

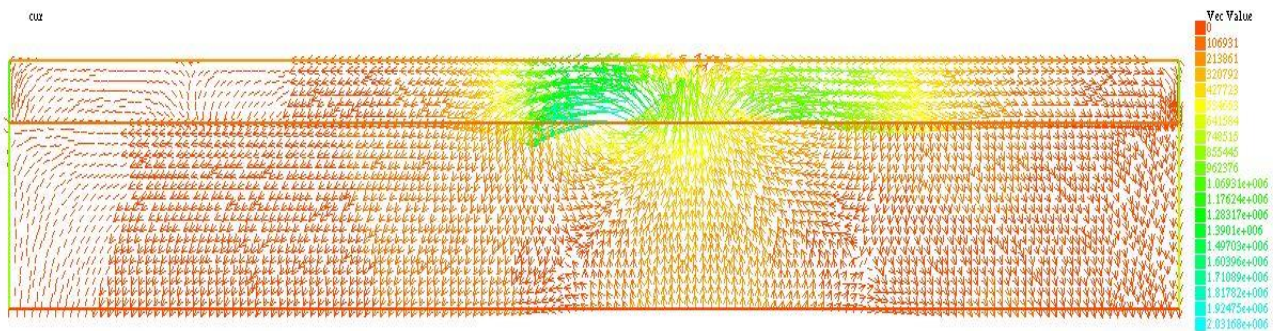


Figure 24: current density profile.

The result is qualitatively in line with the one predicted by Kaldre for a CPS receiving a Gaussian shaped heat load:

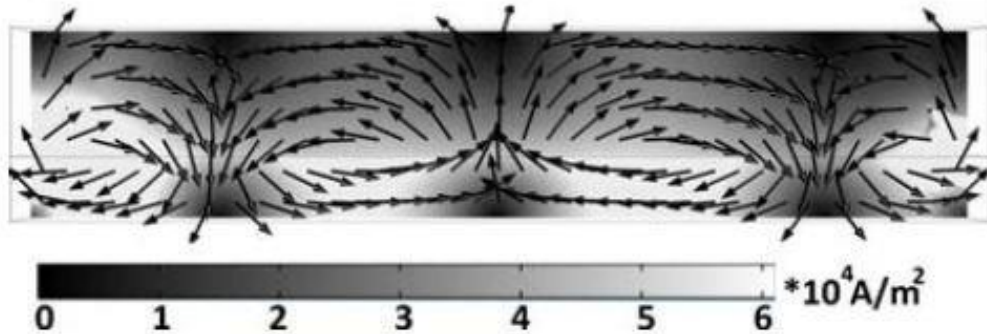


Figure 25: Kaldre results for current density distribution [46].

Being the thermo-electric potential dominant, the current in proximity of the strong temperature gradients assume a direction opposite to them as equation 13 suggest. This is true inside the CPS because its Seebeck coefficient ( $\sim 23\text{V/K}$ ) is higher than the one of the tungsten substrate ( $\sim 8\text{V/K}$ ) therefore its electric potential buildup prevail as the results confirm.

To evaluate the thermo-electric induced pressure from the current density, only the component of the latter interacting with the toroidal magnetic field (that is oriented orthogonally to the section in exam) is chosen. In this way, the  $\mathbf{j} \times \mathbf{B}$  resultant is normally directed towards the CPS surface. Moreover, being  $\mathbf{j} \times \mathbf{B}$  a body force, it is integrated along the CPS thickness to provide the characterizing pressure contribution of the phenomena along the liquid metal surface.

This approach provides the pressure profile sketched in figure 26; if the input parameters specified before are employed.

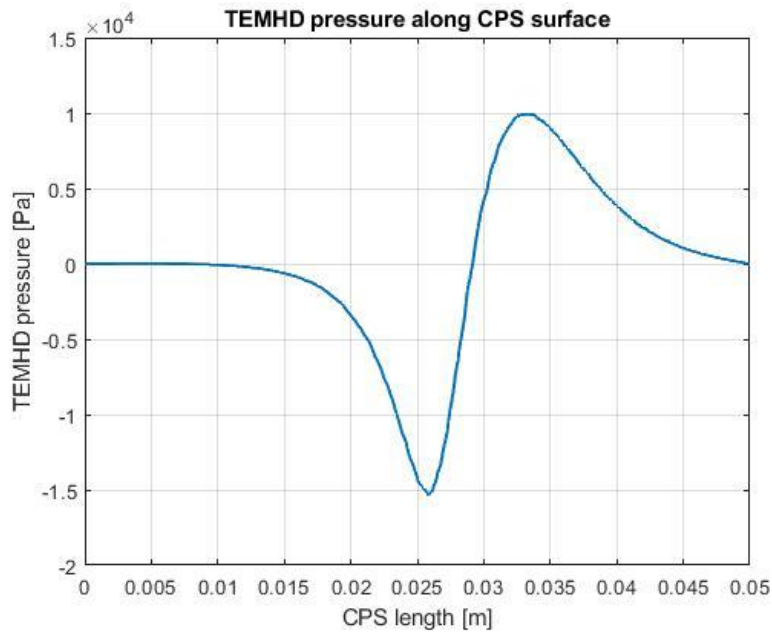


Figure 26: TEMHD pressure along the CPS surface

As figure 24 shows, hazardous current densities, close to  $2 \text{ MA/m}^2$ , are achieved along the interface. These currents remain just in the proximity of the interface experiencing a fast decay to more bearable magnitudes towards the CPS surface. This feature is helpful in order to maintain an overall acceptable pressure on the surface lowering the  $j \times B$  integral value over the liquid metal thickness.

### 6.1.2.2 Grid independence for potential

Below it is briefly assessed the correct mesh choice comparing the number of computational cells with regard the maximum potential registered for both domains, the substrate and CPS.

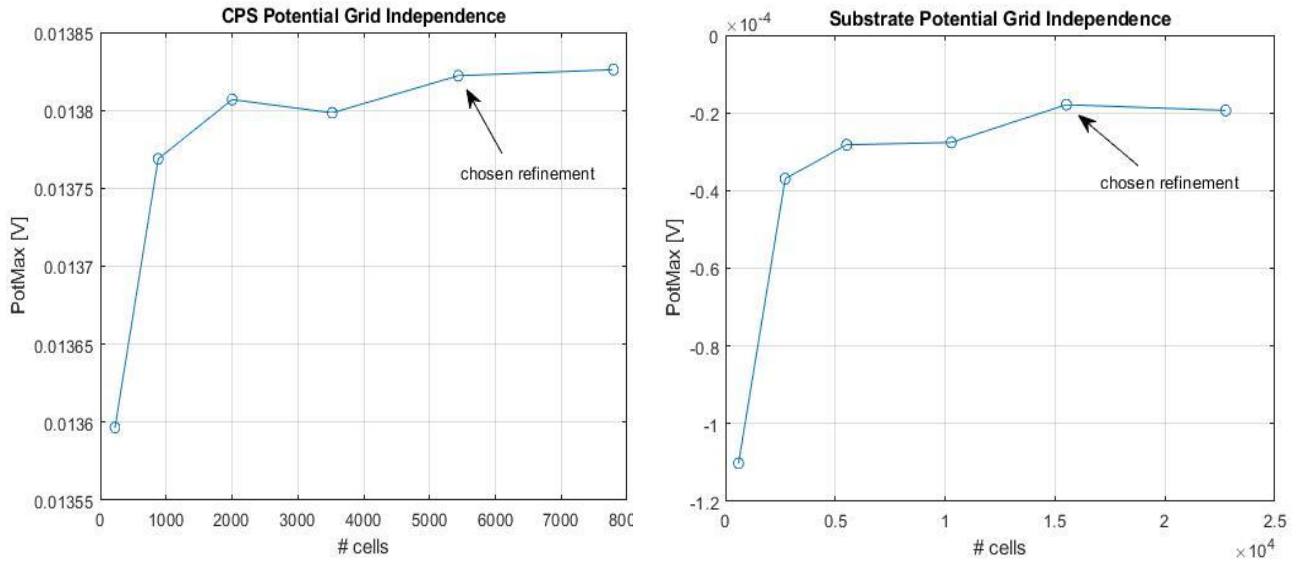


Figure 27: Grid independence respectively of the substrate and CPS discretization

## 7 Results

### 7.1 Parametric study on pressure contribution

For a comprehensive comparison among the pressures involved, each of them is here presented for a sufficiently broad range of independent variables, which is believed to be representative of possible working conditions:

- The capillary pressure is affected by the pore effective radius and the wettability of the liquid-solid interface. Moreover, the temperature affects the surface tension, but in a range of 150 degrees around the reference case of 750 °C the surface tension variation is within 5%, therefore a spectrum is here presented, function of the wetting angle  $\theta$  and the pore radius  $R_{eff}$  values:

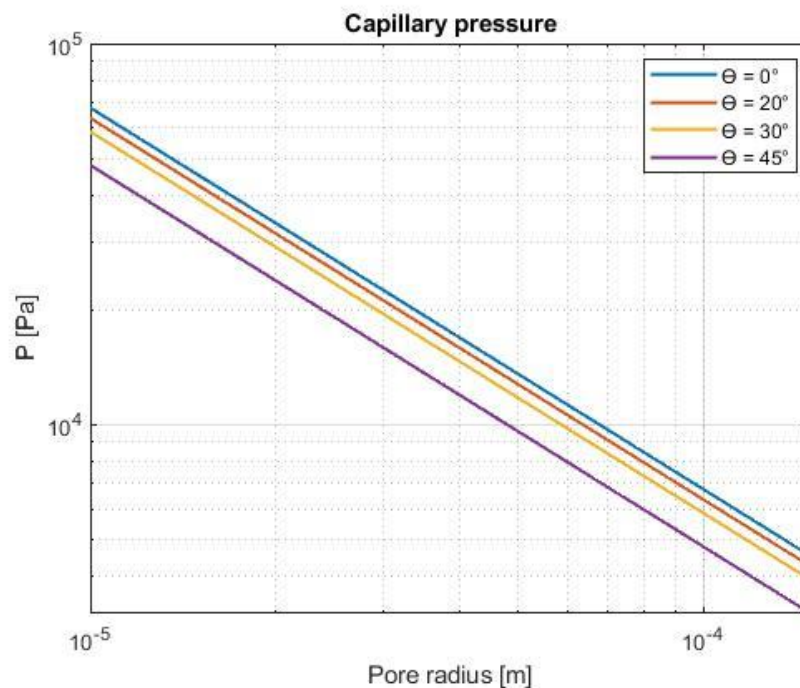


Figure 28: Capillary pressure as a function of pore radius.

Its inverse proportionality with the pore radius determines a range of acceptable radii around just few tens of micrometer in order to compete with the other concurrent

pressures. As far as the wettability is concerned, a wetting angle of  $45^\circ$  determines a decrease in capillary pressure of  $\sim 30\%$ , and a  $30^\circ$  angle affects it for less than  $15\%$ ,  $0^\circ$  wetting angle is achievable by Lithium with the most of construction metals and alloys, Tungsten included; the reference case considering a pore radius of  $15\mu\text{m}$  and a perfect wettability will drive a capillary pressure of  $45\text{ kPa}$ .

- The interface pressure drop shows its only dependence on the saturation pressure that in turn depends on temperature [47], the relation is showed in figure 29:

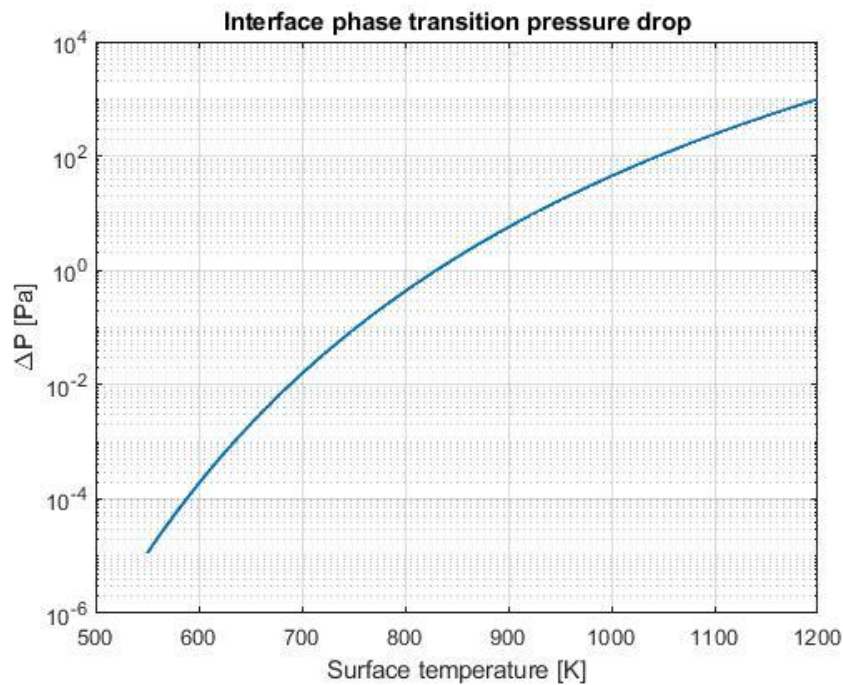


Figure 29: interface liquid-vapor pressure drop.

According to the graph, this contribution barely reaches  $10^3\text{ Pa}$  at  $1200\text{K}$  (where the hottest point on the CPS is around  $1170\text{ K}$ ). As mentioned in section 5.1.2, another relation was found in literature with discrepancies in magnitude and shape compared to the most recent and employed one. A better insight of such formulation has to be

properly addressed and is left for future work. In any case, this is expected to represent a minor contribution to the pressure balance.

- The hydrostatic pressure has a dependence on the CPS height and Li density, since the CPS height does not exceed few millimeters and Lithium density is among the lowest for a metal ( $\sim 450 \text{ kg/m}^3$  at  $\sim 700 \text{ }^\circ\text{C}$ ), this contribution stays rather low compared to the others and remains in the range of several tens of Pascal.

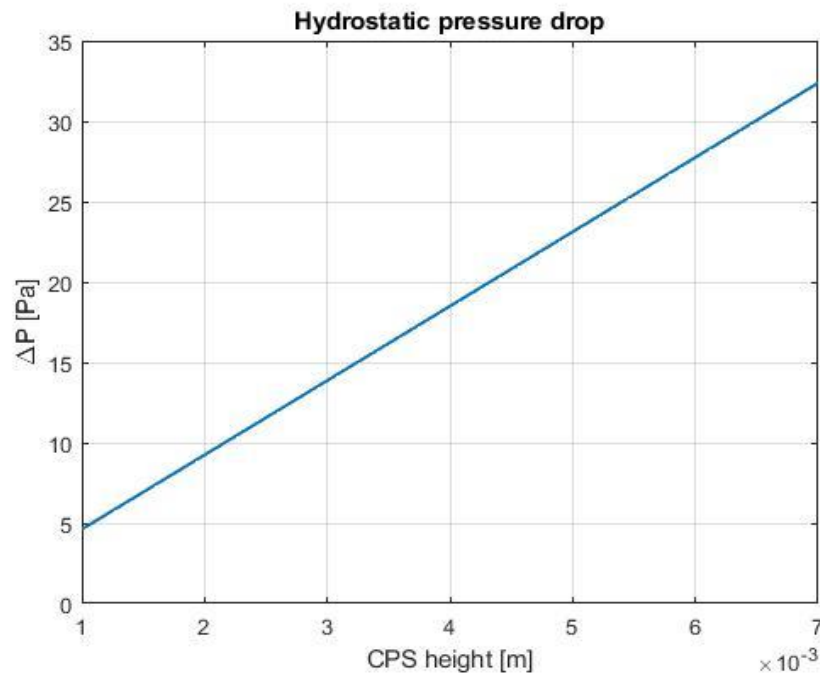


Figure 30: Hydrostatic pressure drop.

- As far as the MHD pressure is concerned Buhler study [32] is exploited. It calculates the pressure drop inside a CPS under magnetic field influence and in Darcy regime and then retrieves the ratio between the two ( $\frac{G_{zz}}{G_{zz,d}}$ ) for a wide range of Hartmann numbers -strengthening the magnetic influence in the pressure drop over the viscous one- as presented in figure 31.

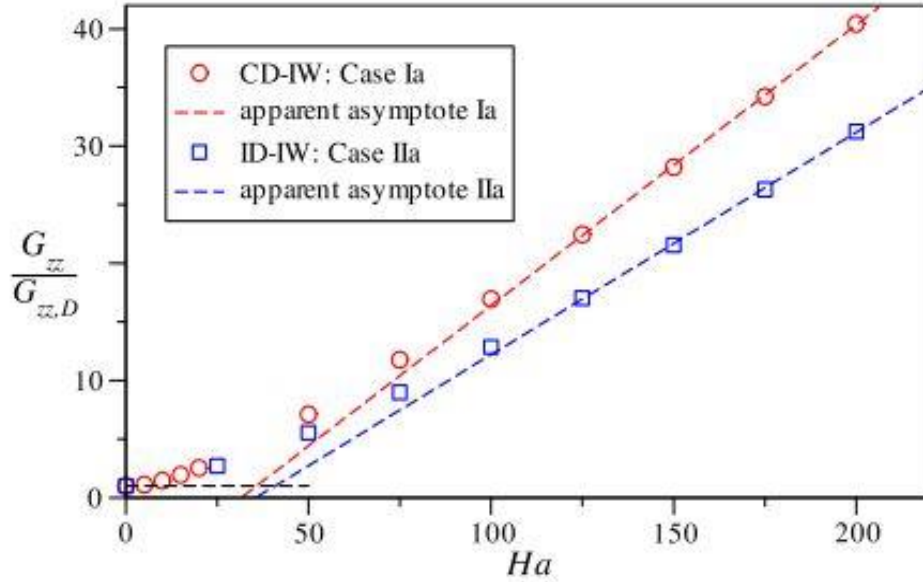


Figure 31:  $\frac{G_{zz}}{G_{zz,D}}$  ratio in case of isolating wire and conducting (Ia) or isolating (IIa) domain for different Hartmann numbers. Subscript zz stand for the pressure drop along flowing direction and D for the Darcy regime only. Adapted from [29]

The similarity with the studied case allows, to relate the viscous drop to the overall hydrodynamic drop at the Hartmann number of interest ( $Ha \sim 14$  rather low thanks to the small pore radius) exploiting the ratio found by Buhler, once known the Darcy pressure drop and the Hartmann number for the considered CPS operation. The  $\frac{G_{zz}}{G_{zz,D}}$  ratio for our case is assumed  $\sim 2$  and is used as a multiplication factor for the Darcy pressure drop found with equation (6) to achieve the total hydrodynamic pressure drop below presented in figure 32 as a function of the permeability and liquid path length from supply point to surface; the results therefore take in account viscous and MHD contribution.

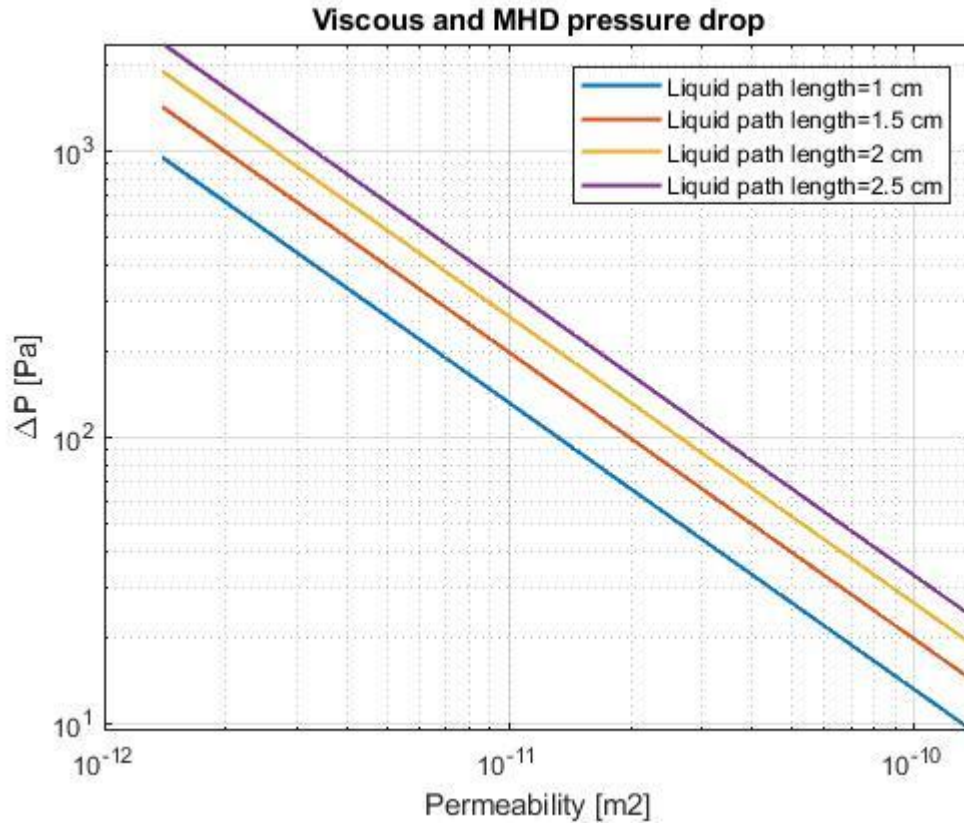


Figure 32: Hydrodynamic pressure drop contribution

Due to the quasi-static regime, the magnitude of this term is slightly above 2 kPa towards the highest scouted ranges. The fixed flowrate in input determined by the evaporative flowrate force the rising of the pressure for finer meshes. The successful mitigation is one of the main reason that CPS design is preferred to a fast flowing one.

- The last term characterized by the TEMHD phenomenon has its main dependence in the temperature profile at the CPS-substrate interface. Therefore, to obtain a preliminary screening for pressure evaluation the chosen parameters to vary are the heat load  $Q''_{div}$  magnitude and the CPS thickness. The  $\Delta P_{temhd}$  is here presented as a pressure profile on the CPS surface following the method described in section 6.1.2.1:

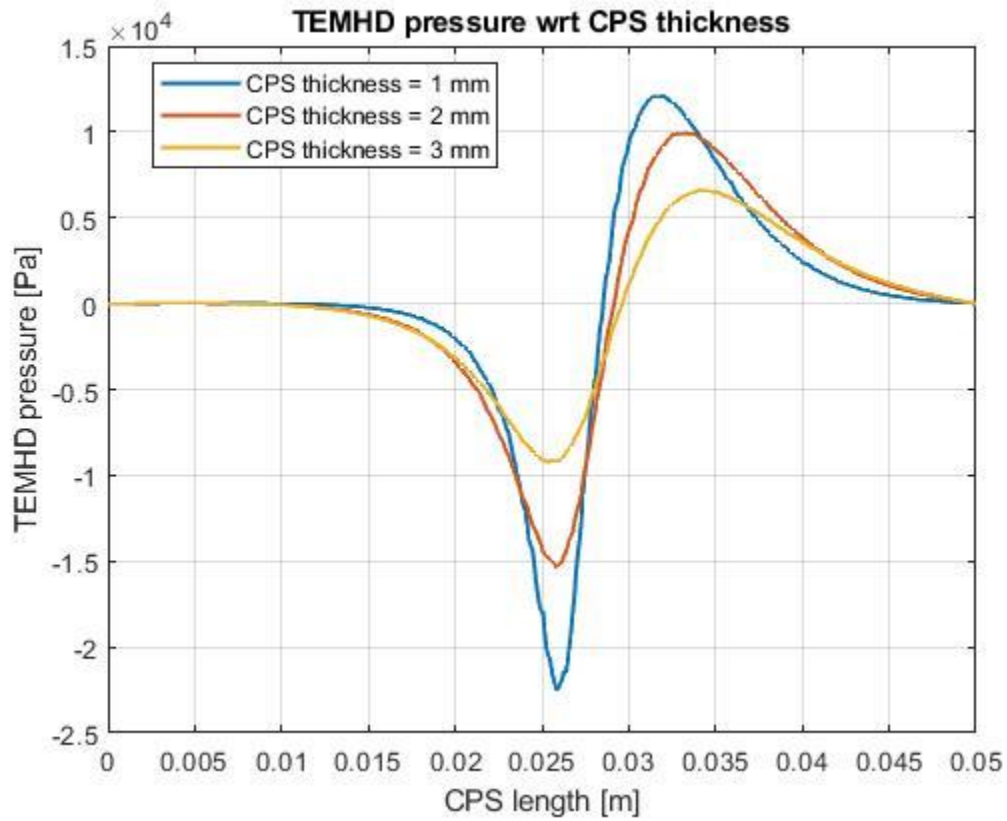


Figure 33: TEMHD pressure along the CPS surface for different thicknesses.

The asymmetry in the heat load is reflected in a higher temperature gradient on the left side of the strike point and therefore a higher current and pressure towards the left of the Separatrix. As expected, the thinner the CPS the harsher the gradient at the interface and the resultant  $\Delta P_{temhd}$ , that still remains in a tolerable range of  $\sim 15$  kPa for a 2 mm thickness, but grows up to threatening values of  $\sim 23$  kPa for a 1 mm thick configuration.

A similar procedure is performed for the heat load, varying  $Q''_{peak}$  in equation (13):

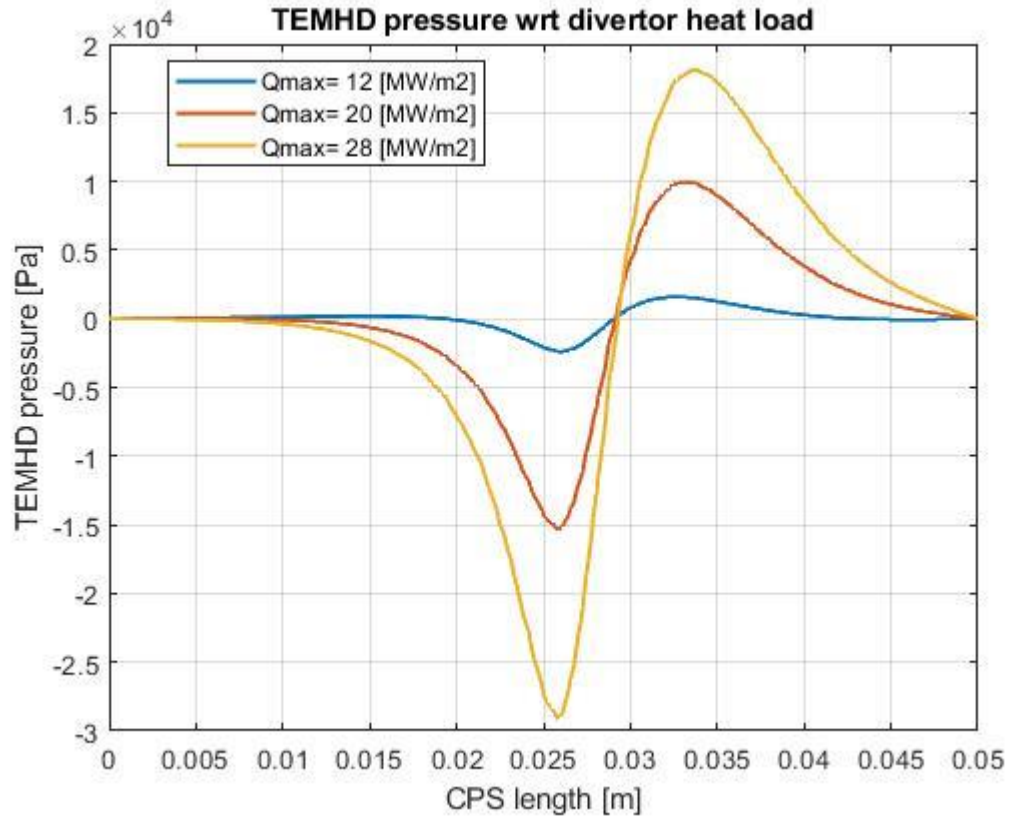


Figure 34: TEMHD pressure along the CPS surface for different power loads.

The phenomenology of the consequences is similar to the one analyzed previously. A larger peak heat load leads to a steeper gradient and higher  $\Delta P_{temhd}$  that reaches almost 0.3 MPa with a maximum load close to 30 MW/m<sup>2</sup>. A peculiarity of this pressure contribution is the opposite direction of application along the CPS surface whether the electric current in it flows poloidally clockwise or counterclockwise. In the first case it pulls the Li into the CPS obstructing the refilling and in the latter pushes it outside, threatening the CPS confinement.

## 7.2 Comparison among pressure contributions for a reference case

In this section the magnitudes of the various pressures contribution are compared in the reference case in order define which contributions are the strongest ones and then highlighting their parameter dependence.

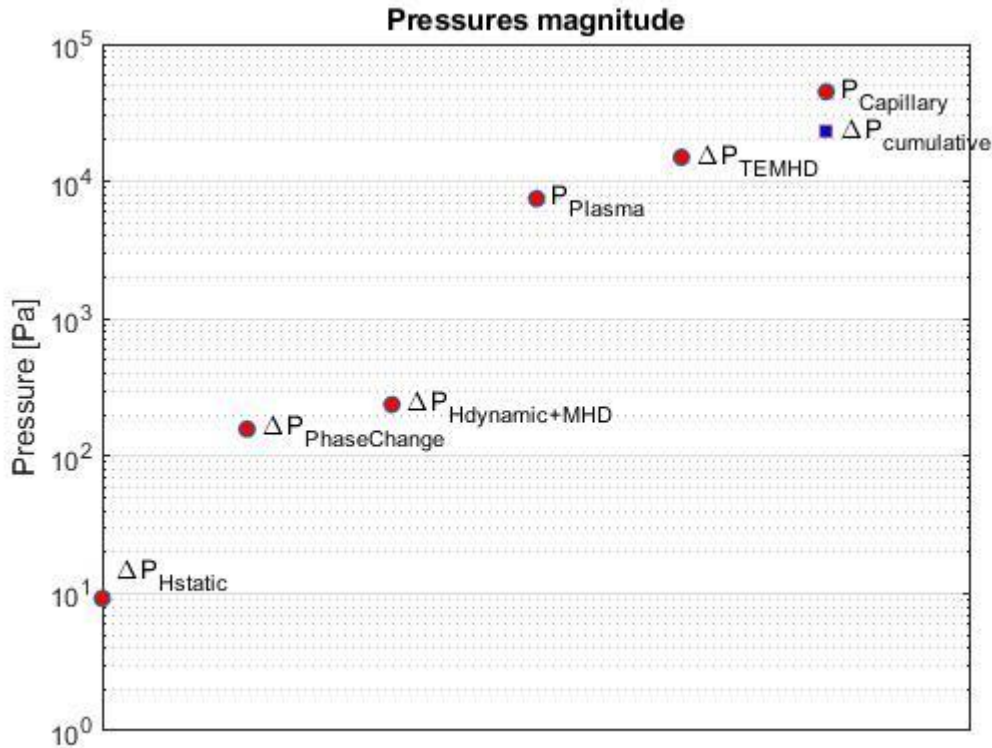


Figure 35: pressures magnitude compared.

Figure 35 displays the magnitude reached by each pressure in the reference case. All the contributions, aside the capillary one and the TEMHD one in the right part of the CPS, act to restrain the liquid Li refilling process favored by the capillary pressure. The  $\Delta P_{cumulative}$  indicated as a square in the plot of figure 35 refers to the highest value achievable considering a cumulative contribution of pressures as if they were all aligned to brake the refill and reaches around half ( $\sim 23\text{kPa}$ ) of the value achieved by the capillary pressure alone ( $\sim 45\text{kPa}$ ). The replenishment is therefore guaranteed in this frame case but probably without a sufficient safety margin over the other forces in play to assess a complete control of the liquid metal

inside the CPS by the capillary force. Further studies are required, especially experimental ones where possible, as it will be specified in section 8. Plasma events harsher than slow transients such as plasma disruptions and ELMs are not considered. Moreover, deterioration of CPS surface properties is likely to happen due to the formation of compounds on the plasma interface threatening further the safety margin. A beneficial reduction of the pore radius can be foreseen up to  $5\ \mu\text{m}$  [49]. This will promote capillary pressures even higher than 0.1 MPa. Even a non-uniform (increasing) pore size in the CPS between the supply point and the surface is a possible countermeasure. Moreover, employing a positive pressure in the lithium supply system can be of help (it is still a free parameter left open to cope with the needs of the design).

As far as the confinement is concerned, only  $\Delta P_{\text{temhd}}$  has a component threatening Li ejection outside the CPS and its magnitude lies between  $10^3$ - $10^4$  Pa, not enough to overwhelm the capillary one. This statements hold unless more severe events, such as ELMs, are considered, since they can bring two main consequences: the first is a larger inhomogeneity and magnitude of the heat flux thus resulting in harsher temperature gradients at the interface and possible spiking of the  $\Delta P_{\text{temhd}}$  contribution; the second is a current associated with the plasma that enters into the CPS and affects again the liquid metal confinement by means of the  $j \times B$  interaction. This phenomena seems to be tamed [50], but further studies are ongoing regarding liquid metal divertor equilibrium and potential instabilities.

Potential fluid regression into the CPS is recovered within the range of millisecond according to [18], if the reference CPS thickness and pore radius are considered.

## 8 Conclusions

This thesis approached the liquid metal divertor problem, considering lithium within a CPS, with a preliminary analysis aimed at defining the main parameter ranges affecting the liquid metal equilibrium inside the CPS with a focus on the thermoelectric component due to the scarcity of material found in literature about such contribution.

The results are encouraging in terms of the possibility of replenishing and confining liquid Lithium by means of the capillary pressure in most cases. This work allowed also the individuation of the TEMHD contribution as the most threatening for the component. Overall, the technology of a liquid metal divertor is growing to a sufficient degree of maturity to be seriously taken in account for the purpose it has been proposed for, although many other aspects have to be investigated and studied in order to provide a deeper insight and assessments of the integrated scenario, especially considering plasma side.

For future developments an experimental approach is highly encouraged to study electric currents generation under inhomogeneous load impinging on the component in order to provide a definitive verification of the TEMHD. As a second issue to address, transient situations from the point of view of a Li filled CPS, and the domain of the CPS can be extended to cover the whole divertor and possibly include also the liquid metal recirculation and supply system. Extending the research with an increased focus on plasma research, coupling a 2D model of the SOL plasma with the CPS response and keeping track of the evaporation and condensation fluxes in the divertor region and on the CPS surface, or in the vapor box (if present) will be necessary for supporting the ongoing design activities. At last, for completeness, keeping in mind the quasi-static regime expected, a 2D fluid dynamic analysis can be performed on the liquid metal in the CPS from supply point to surface to catch in detail phenomena involved and fluid motion field. This, for example, could allow to identify benefits associated with adopting a CPS with variable porosity.

## 9 References

- [1] J. P. Freidberg, *Plasma Physics and Fusion Energy*. Cambridge: Cambridge University Press, 2007.
- [2] G. A. Moses and J. James, “Inertial confinement fusion / James J. Duderstadt, Gregory A. Moses.,” 1982.
- [3] F. Crisanti *et al.*, “The Divertor Tokamak Test facility proposal: Physical requirements and reference design,” *Nucl. Mater. Energy*, vol. 12, pp. 1330–1335, 2017.
- [4] R. Zagórski *et al.*, “The DTT device: Power and particle exhaust,” *Fusion Eng. Des.*, vol. 122, pp. 313–321, 2017.
- [5] F. L. Tabarés, “Reactor Divertor designs based on Liquid Metal Concepts,” 2015.
- [6] R. Albanese and N. Federico, “Guidelines for the design of a tokamak device,” no. June, 2016.
- [7] P. Batistoni *et al.*, “Report of the Ad hoc Group on DEMO Activities,” no. March, 2010.
- [8] Stangeby P. and P. Ghendrih, “The Plasma Boundary of Magnetic Fusion Devices,” *Plasma Phys. Control. Fusion*, vol. 43, no. 2, pp. 223–224, 2001.
- [9] M. Keilhacker, G. Becker, and K. Bernhardt, “Plasma Physics and Controlled Fusion Related content Confinement studies in L and H-type Asdex discharges,” 1984.
- [10] Y. R. Martin and T. Takizuka, “Power requirement for accessing the H-mode in ITER,” *J. Phys. Conf. Ser.*, vol. 123, 2008.
- [11] R. A. Pitts, “Edge physics and plasma-wall interactions,” *Nucl. Fusion*, vol. 2011, no. January, pp. 1–55, 2011.
- [12] R. J. Goldston, “Heuristic drift-based model for the power scrape-off width in H-mode tokamaks,” *38th EPS Conf. Plasma Phys. 2011, EPS 2011 - Europhys. Conf. Abstr.*, vol. 35 1, pp. 385–388, 2011.
- [13] J. H. You *et al.*, “European divertor target concepts for DEMO: Design rationales and high heat flux performance,” *Nucl. Mater. Energy*, vol. 16, no. April, pp. 1–11, 2018.

- [14] F. L. Tabarés *et al.*, “Experimental tests of LiSn alloys as potential liquid metal for the divertor target in a fusion reactor,” *Nucl. Mater. Energy*, 2017.
- [15] M. Ono *et al.*, “Recent progress in the NSTX/NSTX-U lithium programme and prospects for reactor-relevant liquid-lithium based divertor development,” *Nucl. Fusion*, vol. 53, no. 11, p. 113030, 2013.
- [16] T. W. Morgan, D. C. M. Van Den Bekerom, and G. De Temmerman, “Interaction of a tin-based capillary porous structure with ITER/DEMO relevant plasma conditions,” *J. Nucl. Mater.*, vol. 463, pp. 1256–1259, 2015.
- [17] R. E. Nygren and F. L. Tabarés, “Liquid surfaces for fusion plasma facing components—A critical review. Part I: Physics and PSI,” *Nucl. Mater. Energy*, vol. 9, pp. 6–21, 2016.
- [18] F. L. Tabarés, “Present status of liquid metal research for a fusion reactor,” *Plasma Phys. Control. Fusion*, vol. 58, no. 1, 2015.
- [19] D. N. Ruzic, W. Xu, D. Andruczyk, and M. A. Jaworski, “Lithium-metal infused trenches (LiMIT) for heat removal in fusion devices,” *Nucl. Fusion*, vol. 51, no. 10, 2011.
- [20] V. I. Pistunovich *et al.*, “Research of the capillary structure heat removal efficiency under divertor conditions,” *J. Nucl. Mater.*, vol. 233–237, no. PART 1, pp. 650–654, 1996.
- [21] A. Faghri, “Heat Pipes: Review, Opportunities and Challenges,” *Front. Heat Pipes*, vol. 5, no. 1, 2014.
- [22] Y. Nagayama, “Liquid lithium divertor system for fusion reactor,” *Fusion Eng. Des.*, vol. 84, no. 7–11, pp. 1380–1383, 2009.
- [23] M. Ono, M. A. Jaworski, R. Kaita, Y. Hirooka, D. Andruczyk, and T. K. Gray, “Active radiative liquid lithium divertor concept,” *Fusion Eng. Des.*, vol. 89, no. 12, pp. 2838–2844, 2014.
- [24] I. E. Lyublinski *et al.*, “Status of design and experimental activity on module of lithium divertor for KTM tokamak,” *Fusion Eng. Des.*, vol. 88, no. 9–10, pp. 1862–1865, 2013.
- [25] G. F. Nallo *et al.*, “Modeling the lithium loop in a liquid metal pool-type divertor,”

- Fusion Eng. Des.*, vol. 125, pp. 206–215, 2017.
- [26] T. W. Morgan, A. Vertkov, K. Bystrov, I. Lyublinski, J. W. Genuit, and G. Mazzitelli, “Power handling of a liquid-metal based CPS structure under high steady-state heat and particle fluxes,” *Nucl. Mater. Energy*, vol. 12, pp. 210–215, 2017.
- [27] V. A. Evtikhin, A. V. Vertkov, I. E. Lyublinski, B. I. Khripunov, V. B. Petrov, and S. V. Mirnov, “Research of lithium capillary-pore systems for fusion reactor plasma facing components,” *J. Nucl. Mater.*, vol. 307–311, no. 2 SUPPL., pp. 1664–1669, 2002.
- [28] R. L. Givens, S. R. Morrison, W. N. Garrett, and W. B. Hight, *heat pipe design and technology*. 1968.
- [29] A. Faghri, *Heat pipe science and technology*. Washington, DC: Taylor & Francis, 1995.
- [30] I. E. Lyublinski, A. V. Vertkov, and V. A. Evtikhin, “Application of lithium in systems of fusion reactors. 2. the issues of practical use of lithium in experimental facilities and fusion devices,” *Plasma Devices Oper.*, vol. 17, no. 4, pp. 265–285, 2009.
- [31] “G. F. Nallo et al., PFMC conference 2019, Eindhoven (NL) 20-24 May 2019.”
- [32] L. Bühler, C. Mistrangelo, and T. Najuch, “Magnetohydrodynamic flows in model porous structures,” *Fusion Eng. Des.*, vol. 98–99, pp. 1239–1243, 2015.
- [33] J. A. Shercliff, “Thermoelectric magnetohydrodynamics,” *J. Fluid Mech.*, vol. 91, no. 2, pp. 231–251, 1979.
- [34] I. E. Lyublinski, A. V. Vertkov, and V. V. Semenov, “Comparative analysis of the possibility of applying low-melting metals with the capillary-porous system in tokamak conditions,” *Phys. At. Nucl.*, vol. 79, no. 7, pp. 1163–1169, 2017.
- [35] D. Adkins, T. Moss, C. Andraka, N. Andreas, and H. Cole, “An examination of metal felt wicks for heat-pipe applications,” *Conf. Am. Soc. Mech. Eng. Soc. Mech. Eng. Sol. Energy Soc. Int. Sol. energy Conf. Lahaina, HI (United States), 19-24 Mar 1995*, 1994.
- [36] P. Rindt, N. J. Lopes Cardozo, J. A. W. van Dommelen, R. Kaita, and M. A.

- Jaworski, “Conceptual design of a pre-loaded liquid lithium divertor target for NSTX-U,” *Fusion Eng. Des.*, vol. 112, no. 2016, pp. 204–212, 2016.
- [37] J. Safarian and T. A. Engh, “Vacuum evaporation of pure metals,” *Metall. Mater. Trans. A Phys. Metall. Mater. Sci.*, vol. 44, no. 2, pp. 747–753, 2013.
- [38] M. A. Jaworski, N. B. Morley, and D. N. Ruzic, “Thermocapillary and thermoelectric effects in liquid lithium plasma facing components,” *J. Nucl. Mater.*, vol. 390–391, no. 1, pp. 1055–1058, 2009.
- [39] R. A. Pitts *et al.*, “Physics conclusions in support of ITER W divertor monoblock shaping,” *Nucl. Mater. Energy*, vol. 12, pp. 60–74, 2017.
- [40] S. Carli, “SOLPS-ITER simplified heat transfer model for plasma facing components,” 2017.
- [41] J. H. You *et al.*, “European DEMO divertor target: Operational requirements and material-design interface,” *Nucl. Mater. Energy*, vol. 9, pp. 171–176, 2016.
- [42] R. Wenninger *et al.*, “Advances in the physics basis for the European DEMO design,” *Nucl. Fusion*, vol. 55, no. 6, 2015.
- [43] G. G. Van Eden, T. W. Morgan, D. U. B. Aussems, M. A. Van Den Berg, K. Bystrov, and M. C. M. Van De Sanden, “Self-Regulated Plasma Heat Flux Mitigation Due to Liquid Sn Vapor Shielding,” *Phys. Rev. Lett.*, vol. 116, no. 13, 2016.
- [44] G. F. Nallo, “PFMC and ISCA conference.”
- [45] Y. F. Fan *et al.*, “A new method for calculating thermoelectric current during the solidification of alloys To cite this version : HAL Id : hal-01331678,” 2016.
- [46] I. Kaldre and O. Lielausis, “ROLE OF THERMOELECTROMAGNETIC FORCES IN CAPILLARY POROUS SYSTEMS PROPOSED FOR LIQUID METAL COOLING OF FUSION REACTOR COMPONENTS.”
- [47] H. W. Davison, “Compilation of thermophysical properties of liquid lithium,” *Natl. Aeronaut. Sp. Adm.*, no. July 1968, 1968.
- [48] D. Lide, “CRC Handbook of Chemistry and Physics,” 1995.
- [49] V. A. Evtikhin *et al.*, “Lithium divertor concept and results of supporting experiments,” *Plasma Phys. Control. Fusion*, vol. 44, no. 6, pp. 955–977, 2002.

- [50] M. A. Jaworski *et al.*, “Macroscopic motion of liquid metal plasma facing components in a diverted plasma,” *J. Nucl. Mater.*, vol. 415, no. 1 SUPPL, pp. S985–S988, 2011.

## Acknowledgements

In this section people who contributed to the development of this thesis and supported me in the process are mentioned:

Before anyone else Ph.D. student Giuseppe Francesco Nallo for the wisdom shared with me about fusion relevant arguments, for your valuable advices on writing, useful discussion, and the anecdotes on your meetings with researcher like Rind and Jaworski; you have always be welcoming to me, every time I knocked on your doorstep a bombastic “AVANTI” followed. Prof. Fabio Subba for approaching me to the thesis subject and the precious help with the model specially for the electric potential distribution.

Dr. Antonio Froio for his availability about FreeFem coding doubts.

A special thanks to doctor Enrica for always being on my side, she is the main reason to improve on myself.

The “fino alla fine” fellowship, Gabriele and Maurizio, for having assisted me till to the end and beyond.

My parents to have made it possible and my brothers for being an example.

My friends Cuni, Kikko, Riky, Paske, Verg and Teo to have made these years *great years*, from the top of the mountains to the basket fields, from the “HTJ” to the climbing gym, from the soccer pitch to the chess board, thank you all.